NTNU
Norwegian University of
Science and Technology

Characterization of the Electrical Resistivity and Water Sorption Properties of a Semiconducting Swelling Tape

Maria Nicte Polanco Olsen

Chemical Engineering
Submission date: June 2018
Supervisor: Brian Arthur Grimes, IKP

Norwegian University of Science and Technology
Department of Chemical Engineering

Preface

This master thesis is the final project of the course TKP4900 provided by the joint programme MSPOLYTECH, given at The Norwegian University of Science and Technology (NTNU) and Royal University of Stockholm (KTH). The experimental work was performed at SINTEF Energy Research.

Most of all I wish to thank my supervisor Torbjørn Andersen Ve at SINTEF Energy Research for supervision, guidance and educational work during this project. I would like to thank Sverre Hvidsten at SINTEF Energy Research for great inputs on experimental method and overall supervision. Thanks to Knut Brede Liland and Hallvard Faremo for great discussions and help, and thanks to Erik Bjerrehorn, Morten Flå, Oddgeri Rokseth for all technical help.

At last I would like to thank my supervisor at the Dept. of Chemical Engineering at NTNU, Brian A. Grimes and Mikael Hedenqvist at the Dept. of Polymeric Materials at KTH for supervision and support.

Abstract

In presence of moisture and localized field enhancements water trees might develop within the polymeric insulation of HV subsea power cables. Water trees tend to grow unnoticeable and deteriorate the insulation properties with time. The humidity within the insulation can efficiently be reduced through the application of semiconducting swelling tapes. Semi conducting swelling tapes provide a unique combination of electrical conductivity and a large water retention capacity. This is attributed to the presence of conductive carbon black (CB) and superabsorbent polymer (SAP) particles, respectively.

To understand the mass transport properties of water vapor within a swelling tape, transport coefficients were determined. The sorption of water vapor revealed concentration dependent transport coefficients and a general increase in diffusion and solubility with increasing water activity. This was attributed to the hygroscopic and polyelectrolyte properties of the SAP components and resulted in an increase in diffusivity by a factor of 100, when increasing the relative humidity (RH) from 7 to 65 %. At higher water activity, it was assumed that the formation of immobile water clusters reduced the diffusion of water vapor. Several sorption modes were suggested for the sorption behaviour of the tape between 10 to 80 % RH.

The introduction of conductivity within the tape reduces potential differences throughout several cable layers and subsequent field enhancements. However, conductivity and water sorption properties of the semi-conductive swelling tape can be altered by mechanical compressions, exerted by surrounding cable components. The electrical resistivity of a humid swelling tape under load was therefore determined. Due to the anisotropy of the tape, electrical resistivity measurements were performed across (radial direction) and along with (axial direction) the tape. The radial and axial directions of the tape were dominated by the presence of SAPs and CBs, respectively. A significant reduction in radial resistivity of the tape was observed when increasing the humidity from 40 % to 60 % RH. The resistivity decreased by a factor of 100. No significant effect of compression was observed, but the tape showed a decreasing trend in resistivity with increasing compression. At 60 % RH radial resistivity approached axial resistivity, and the influence of SAPs is reduced. The axial resistivity was around 18 Ωcm. The axial resistivity of the tape was less affected by humidity and compression than the radial resistivity.

Ageing reveal deterioration of swelling height, but had no influence on tape resistivity.

Table of Contents

List of Figures

List of Tables

Abbreviations

EU	European Union
HV	High Voltage
XLPE	Crosslinked poly(Ethylene)
SAP	Superabsorbent Polymers
CB	Carbon Black
T_g	Glass Transition Temperature
T_m	Melting Temperature
RH	Relative Humidity
BET	Brunauer-Emmet-Teller
TMTPA	4,4’,4’’, Trimethyltriphenylamine
ISO	International Organization for Standardization

Symbolic List

M_c	Molecular weight of crosslinks, [g/mol]
M_n	Molecular weight of polymer chains, [g/mol]
V_1	Molar volume of solvent, [m^3]
X	Interaction parameter
q	Swelling ratio [V_∞/V_0]
ρ_0	Polymer density at dry state [kg/m^3]
M	Mass, [kg]
M_∞	Mass at equilibrium, [kg]
D	Diffusion Coefficient, [m^2/s]
C	Concentration, [kg/m^3]
C_∞	Concentration at equilibrium, [kg/m^3]
C_0	Initial bulk concentration, [kg/m^3]
C_1	Initial surface concentration, [kg/m^3]
l	Sample thickness, [m]
G	Dimensionless parameter
S	Solubility, [kg/m^3Pa]
P	Permeability, [kg/msPa]
p	Gas pressure, [Pa]
p_w	Vapor pressure, [Pa]
a_w	Water activity
ΔH_{vap}	Enthalpy of vaporization, [kJ/mol]
R	Gas constant, [J/Kmol]
T	Temperature, [K]
U	Voltage, [V]
R	Resistance, [Ω]
I	Current, [A]
ρ	Resistivity, [Ωm]
σ	Conductivity, [S/m]

1. Introduction

1.1. Energy and Electrification

Over the past century, energy has developed into an inevitable part of human life and has become crucial for the development of modern societies. Its major impact within our lives is reflected in everyday household activities such as cooking, cleaning and heating, and sectors such as transportation, agriculture and industry [1]. Accessible energy provide wealth, welfare and economic development, but challenges regarding sufficient supply and environmental sustainability increases with growing demand [2].

One of the largest contributions to sufficient and sustainable energy supply is a shift towards electrification [3]. By 2040, the International Energy Agency has estimated a 30 % rise in world primary energy consumption compared to 2016, whereas almost half of the demand will be covered by electricity. In addition, the total share of electric power generated from renewables is reaching up to 80 % in the EU and up to 40 % worldwide [4, 5]. The future scale of electricity needs and its major contribution to decarbonizing, reduction in greenhouse gas emissions and improved living, makes electricity supply crucial for years to come.

1.2. Subsea Power Cables and Transmission

For the generated electricity to be transmitted between overseas countries and territories, near shore islands or offshore installations, power grids are interconnected. Interconnections of autonomous power grids allow for sufficient and stable power supply, optimized resource utilization and increased share of sustainable energy throughout the entire network [6].

Though overhead lines can be used for overseas crossings up to 3 km, subsea power cables are often preferred. This is mainly due to their invisibility and their reduced restrictions and disruptive impact from the surroundings. In addition, maintenance-free subsea power cables provide safe and secure transmission with operational lifetime costs that can be lower than for overhead lines [6].

1.3. Water Tree Formation

The development of maintenance-free subsea power cables is highly related to the condition of the insulation. In high voltage (HV) XLPE-insulated power cables, the formation of so-called water trees might occur within the polymeric insulation. Water trees are branched-like water-channels, schematically represented in figure 1, which can deteriorate the characteristic insulation properties with time. Their initiation is caused by the synergic effect of humidity (condensation of vapor) and localized electrical field enhancement, commonly described by mechanical and electrochemical mechanisms. After initiation they tend to grow unnoticeably. If growth is allowed to continue, the breakdown strength and lifetime of the insulation will be drastically reduced [6-8].

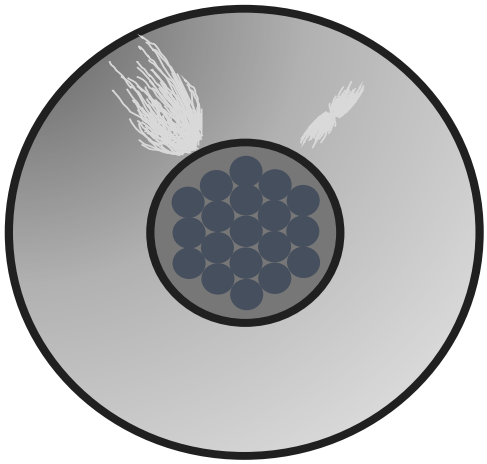

Figure 1. Representation of vented (left) and bow-tie (right) water trees within the insulation [8]

1.4. Semi-Conductive Swelling Tapes

There are several ways to prevent moisture within solid insulation systems. Whereas triple-extrusion processes and dry curing provide initial dry insulation conditions, a metallic sheath prevents radial water ingression during operational lifetime. Though these approaches are highly efficient, they do not prevent migration of water after a cable fault [6]. Longitudinal water ingression and subsequent radial diffusion after cable fault can be reduced by the incorporation of water blocking swelling agents. Swelling agents consist of polymeric

hydrogels or super-absorbing polymers (SAP), capable of absorbing large amounts of water. Their unique combination of hygroscopicity, flexibility and crosslinks enable them to swell and retain moisture without dissolving, reducing further water migration into the insulation [9].

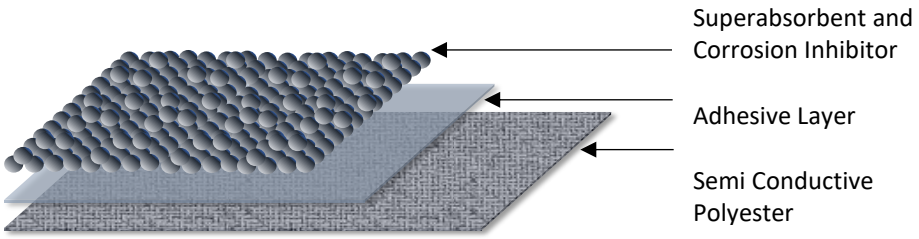

Figure 2. Characteristic layers of a woven, single sided swelling tape

In cable manufacturing, facilitated control and handling of SAP particles can be provided by application of swelling tapes. A schematic representation of a tape can be seen in figure 2. Swelling tapes are complex materials, made specifically for their position and function within the cable. Through adhesion of SAP particles onto a textile fabric, swelling tapes are easily are wrapped around the conductor core or insulation screen (see figure 3) [6]. They can be woven or non-woven, double or single sided and contain corrosion inhibitors and antioxidants. For HV applications, semi-conductive tapes are provided through coatings of conductive carbon black (CB). The introduction of conductivity equalizes potential

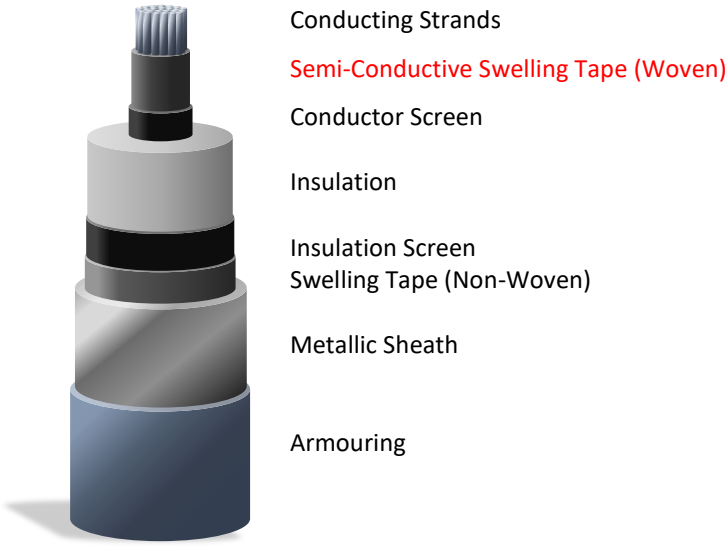

Figure 3. Schematic representation of a subsea power cable and positioning of a semi-conductive swelling tape (red)

differences throughout the cable and reduces possible formation of localized field enhancements.

1.5. Problem Description and Objective

The unique combination of water retention and conductivity represents the fundamental properties of semi-conductive swelling tapes. However, their positioning within subsea power cables makes them exposed to mechanical compression, exerted by the surrounding cable components, and ageing by elevated temperatures near the conductor core. This is of interest, due to the fact that compression and ageing may alter or deteriorate the electric and water blocking features of the tape. Until now, little or no research has been done on the synergic and individual effect of compression and humidity on the tape's electrical response, and little is known of the ageing characteristics of the tape. It is therefore considered necessary to understand these relations, in order for future power cables to be optimized.

In this report, the effect of water concentration and mechanical compression on the electric resistivity of a semi-conductive swelling tape will be investigated. An image of the tape can be seen in figure 4. The report will reveal the mass transport properties of water vapor within the tape which will be related to the resistivity of a humid tape under load. This will be presented in chapter 4. Customized measuring techniques for the characterization will be presented in chapter 3, and their validation will be analyzed. Ageing and its effect will be investigated in terms of electrical resistivity and swelling height in section 4.4. The goal of the characterization will be an improved understanding and knowledge of semi-conductive swelling tapes in relevant operational conditions.

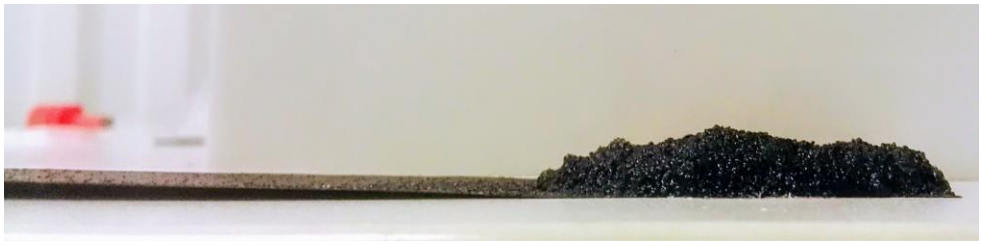

Figure 4. Swelling tape where the right side is swollen in deionized water

2. Theoretical Background

2.1. Structure and Properties of Polymers

Polymers are large macromolecules composed of several smaller chemical units or *monomers*. The monomers are bounded by strong primary bonds into polymeric chains of high molar mass, which dominates the thermal stability and chemical reactivity of the molecule. Their structure is described by regularity and arrangement of polymer chains and formation of amorphous and crystalline segments [10].

Long, irregular and bulky chains have the tendency to entangle and randomly orient themselves into amorphous polymer structures. Amorphous polymers are recognized as brittle, hard and transparent in their "glassy" state. Above the glass transition temperature (T_g), they experience a second order phase transition or relaxation. Relaxation allows for enhanced chain mobility, molecular diffusion and flow, and transforms brittle polymers to rubbery, elastic masses [11].

Compared to purely amorphous polymers, polymers such as fibrous polyesters, are highly crystalline [12]. The introduction of crystalline segments reduces the distinct changes in polymer properties at T_g. Instead, they become leathery before they melt and relax at T_m; the temperature disrupting the crystalline structure. Polymeric crystallites are composed of aligned chains which are densely packed into organized segments. The close packing enhances interacting forces and reduces chain mobility, providing materials which are dense, tough and opaque [10].

Crosslinked polymers are characterized by the presence of crosslinking chains which connects the main polymer chains into one large and insoluble network. The crosslinks are composed of strong covalent bonds (may also be ionic or physical), which restrict chain mobility and prevent deformation of materials under load. Between the crosslinks, however, flexible chains are present. Dependent on the degree of crosslinking, these chains allow for volume expansion, segmental mobility and may cause the material to flow at appropriate temperatures. This makes lightly crosslinked polymers rubbery above their T_g. For highly crosslinked polymers or thermosets, the flexibility of chains are reduced, and the material remains rigid over a broad range of temperatures [10].

2.2. Swelling in Hygroscopic SAPs

Superabsorbent polymers differ from other hygroscopic absorbents such as cotton and wood pulp by the presence of crosslinks. Crosslinks keep the molecule from dissolving while the flexible, hydrophilic chains allow for enhanced volume expansion. As a small, rigid SAP particle becomes solvated by water it gradually changes to a soft, swollen gel.

Crosslinked, partially neutralized poly(sodium acrylate) is the principal superabsorbent polymer in use [9]. A representation of the polymer network can be seen in figure 5. Superabsorbent polymers absorb water and aqueous fluids by means of entropic and energetic interactions made possible by simple mixing. Upon mixing, hydrophilic groups are solvated by water through the formation of hydrogen bonds and the entropy of the system increases. However, the energetic and entropic mechanisms are largely overshadowed in magnitude by the presence of ionic charges spaced along the polymer chains and their counterions. The presence of ions introduces strong ionic interactions which enhances absorption of water [9].

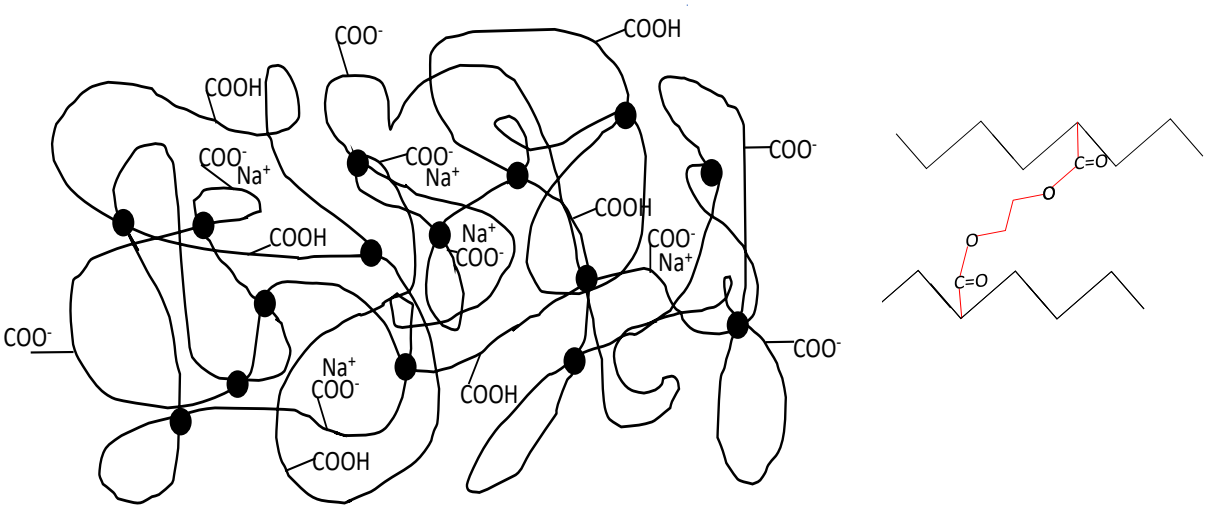

Figure 5. Schematic representation of partly neutralized crosslinked poly(sodium acrylate) network (left) with ionic components.[12] The dots represent crosslink or junction sites in the network. On the right is an enlarged representation of crosslinking chains M_c (red), connecting the backbone chains M_n (black)

In reaction with water, ions become strongly solvated by water through strong ion-dipole interactions. If the concentration of ions outside the SAP particle is low, an osmotic pressure is created, and water begins to diffuse towards the polymer bulk. This inequality of chemical potential of water and ions inside and outside the gel is the main driving force for swelling. As water continues to enter the polymer structure, sodium ions lose their fixation to the main chain and carboxylate ions tend to repel each other. The repulsions cause polymeric chains to extend through changes in configurational states, which in turn increases the solvating volume. As a consequence, even more water is allowed to be absorbed. With sufficient water concentration, chains extend as a necessary consequence of the volume expansion. This exerts a force which at some point is equalized by forces arising from osmotic pressure. At this point, the SAP reaches maximum swelling capacity [9].

2.3. Variables in the Swelling Analysis

There are several variables affecting equilibrium swelling capacity of the polymer. The solvating molecules have a large influence on equilibrium swelling, provided by the interaction parameter X and the molar volume V_1. The molecular weight of the polymer backbone M_n and average molecular weight of chains M_c between crosslinks also affects swelling capability and are determined by polymerization conditions. Contributions to equilibrium swelling ratio q can be seen in eq. 1:

$$q^{5/3} = \frac{\left(\frac{1}{2} - X\right) 2M_c}{V_1 \rho_0 v^{2/3}(1 - 3M_c/M_n)} \qquad (1)$$

where v depends on polymer concentration at the time of preparation and ρ_0 is the density of dry polymer. q is defined as the swelling ratio from reference state volume to the volume at equilibrium through: $q = \frac{V_{eq}}{V_0}$. The degree of neutralization (Na^+) alters the concentration of ions inside the gel and increases the swelling capability. Ionic effects provided by the polymer backbone are neglected in eq. 1, but can be accommodated for by using an effective value of X [9]. Large swelling capability is additionally achieved through low crosslink density which increases molecular weight of crosslinking chains (M_c) [13].

2.4. Network Compressibility

When swollen SAPs are subjected to a mechanical stress they may deform or strain. Deformation increases the free energy and chemical potential in the system, causing water to diffuse from the gel to the surroundings. This lowers the swelling capability of the gel. The magnitude of deformation, and subsequent degree of deswelling, is related to the modulus of elasticity, which refers to the recovered strain after stress removal. High modulus is provided through high crosslink density, which reduces deswelling under load [9].

2.5. Effect of Moisture

Increasing moisture content has proven to change the state of superabsorbent polymers in the same manner as temperature increase (see section 2.1). At certain moisture contents the T_g of SAP is reduced through plasticization by solvents, comparable to relaxation processes in amorphous and crystalline segments. Plasticization by moisture enhances molecular mobility and diffusion rates. However, increasing water concentrations promote adverse effects on modulus [9, 14, 15].

2.6. Diffusion of Water Vapor

Due to the hygroscopicity of super-absorbents, water uptake in swelling tapes is assumed to be dominated by the mass transport properties of the SAPs. Compared to traditional absorbent materials where gas or liquid is taken up by flow or convective mechanisms, water absorption in SAPs function by means of diffusive mechanisms. Diffusion is the kinetic contribution to mass transport phenomena. The process is caused by differences in chemical potential, and matter is transferred from average positions in space toward regions of lower activity [9].

The simplest way of describing mass transport of vapor through a polymer is via Fick's first law:

$$J = -D\frac{\partial C}{\partial x} \qquad (2)$$

The equation states that the flux J of a gas through an area perpendicular to the direction of diffusion is proportional to the concentration gradient $\frac{dC}{dx}$ [16]. The constant of proportionality is known as the diffusion coefficient, D. For ideal systems the diffusion coefficient is independent of concentration. This provides constant diffusion coefficients and Fick's second law can be applied. Fick's second law for diffusion in one dimension is given by:

$$\frac{\partial C}{\partial t} = -D\frac{\partial^2 C}{\partial x^2} \tag{3}$$

where changes in concentration is a function of diffusing path length x and time t [17]. After a certain time, steady states are reached, and the concentration remains constant.

2.7. Diffusion Coefficient Determination

The diffusion coefficient in non-steady states can be determined by sorption of a gas within a polymeric. If the initial bulk concentration of the film is C_0 and the surfaces of the film are kept at constant concentration C_1, Fick's second law yields the following solution:

$$\frac{C - C_0}{C_1 - C_0} = 1 - \frac{4}{\pi}\sum_{n=0}^{\infty}\frac{(-1)^n}{2n+1}e^{\frac{-D(2n+1)^2\pi^2 t}{4l^2}}\cos\frac{(2n+1)\pi x}{2l} \tag{4}$$

when assuming initial and uniform boundary conditions:

$$C(0 < x < l) = C_0 \tag{5}$$

$$C(x = 0) = C(x = l) = C_1 \tag{6}$$

[17]. The solution implies diffusion in one direction over the film thickness l, and negligible amount of diffusing substance entering through the edges.

An integration of eq. 4 over the thickness of the film gives the relation between the absorbed mass of water within the film at any given time $M(t)$ and the amount of water at equilibrium M_∞ (t=∞), presented as the dimensionless parameter G:

$$G = \frac{M(t)}{M_\infty} = 1 - \frac{8}{\pi^2}\sum_{n=0}^{\infty}\frac{1}{(2n+1)^2}e^{-\frac{D(2n+1)^2\pi^2 t}{l^2}} \qquad (7)$$

which can be approximated to the equation:

$$G = 1 - e^{-7.3\left(\frac{Dt}{l^2}\right)^{\frac{3}{4}}} \qquad (8)$$

[17]. When defining C_∞ as amount of water at equilibrium pr. volume dry sample [kg/cm^3], G is related to the water concentration at any given time $C(t)$ through:

$$C(t) = C_\infty G(t) + C_0\big(1 - G(t)\big) \qquad (9)$$

where C_0 is the initial bulk concentration? The diffusion coefficient is determined from the parameter G. Water concentrations will approach equilibrium concentrations when $t = t_\infty$.

2.8. Diffusion Coefficient Estimation

When assuming constant sample volume and Fickian diffusion, an apparent diffusion coefficient can be estimated by plotting $\frac{M(t)}{M_\infty}$ from experimental sorption data versus time [18]. The initial slope of the curve gives the linear relation:

$$\frac{M(t)}{M_\infty} = \frac{4}{\sqrt{\pi}}\sqrt{\frac{Dt}{l^2}} \qquad (10)$$

or

$$D = \frac{0.049}{t_{0.5}/l^2} \qquad (11)$$

where $\frac{M(t)}{M_\infty}$ = 0.5 and $t = t_{0.5}$ at 50 % saturation [18]. A typical curve can be seen in figure 6 with corresponding variables found in eq. 10 and 11.

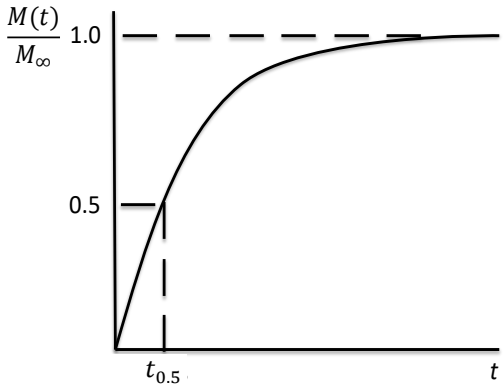

Figure 6. Estimation of diffusion coefficient at 50 % saturation

2.9. Mechanisms of Diffusion

Diffusion in polymers is highly dependent on the size, shape and polarity of the diffusing substance and the state and structure of the polymeric mass. When water molecules diffuse towards the polymer bulk, polymer chains needs to move cooperatively in opposite direction [9]. The ease of chain movement is related to e.g. degree of crosslinks, crystallinity and glassy/rubbery states. This provides distinct categories for diffusion [19]:

- Fickian: diffusion is slow compared to chain mobility. Sorption boundary conditions are independent of time and do not depend on swelling kinetics. Fickian diffusion tend to be the case for polymers above their T_g, where relaxation and plasticization enhances chain mobility;
- Non-Fickian: diffusion is fast compared to chain mobility and sorption is highly related to swelling kinetics;
- Anomalous diffusion: diffusion occurs simultaneously with chain relaxation. Sorption is influenced by the geometrical structure of polymers and the presence of micro voids;

Within SAPs, the diffusion of small water molecules is fast compared to the mobility of large, crosslinked chains causing non-Fickian diffusion. For non-Fickian, diffusion coefficients are generally concentration dependent, $D(C)$, and diffusion becomes a function of concentration and time. Enhanced understanding of the mechanisms involved is provided by the relation:

$$\frac{M(t)}{M_\infty} = kt^n \qquad (12)$$

where k is a rate constant. When $n = 0.5$, Fickian diffusion can be assumed, whereas $n = 1$ indicates non-Fickian diffusion. Intermediate values indicate anomalous diffusion and n is given as: $0.5 < n < 1$ [19, 20].

2.10. Solubility of Swelling Tapes

Whereas diffusion is related to the kinetics of molecules, solubility is a thermodynamically driven parameter, commonly described by sorption of a gas within a material. The sorption term involves both adsorption, absorption, occupation of specific sites and clustering of aggregates. At a given temperature the local concentration C of a gas within a polymer can be related to the partial pressure of the gas p through:

$$C = S(C)p \qquad (13)$$

where $S(C)$ is the concentration dependent solubility coefficient. For a binary polymer-solvent system, the size and nature of interacting forces dominate the degree of solubility at equilibrium. The solubility coefficient is therefore specific for each set of interacting molecules and is highly related to polymer state, structure and thermal history [19]. This provides different quantities of solute molecules and different modes of sorption.

For ideal systems the solubility coefficient S_d is independent of concentration and commonly referred to as Henrys constant, k_d. At a given temperature, this provides a linear relation between the penetrant concentration and the partial pressure of the solvating gas. The sorption mode can thus be described by Henry's Law:

$$C_d = S_d p \qquad (14)$$

[18, 19] where C_d is the saturation concentration. The gas is assumed to be randomly distributed within the polymer matrix and neither polymer-solvent or solvent-solvent interactions are stronger than the interactions between the chains. This sorption mode provide isotherms as represented in figure 7A [18, 19].

For gases dissolving in glassy polymers (below T_g), an additional Langmuir type of sorption often occurs simultaneously with Henry sorption mechanisms. This results in a dual sorption mode. Langmuir sorption concerns gas occupation of specific sites e.g. polar segments, micro-voids or holes within the polymer structure and predominance of solvent-polymer interactions. After occupation of specific sites, a small amount of gas may solubilize. This causes the concentration to increase sharply with increasing water activity before stabilizing at saturated conditions. The resulting sorption provides isotherms as in figure 7B. From Langmuir sorption isotherms the concentration of a gas can be found through:

$$C_h = \frac{c_h' bp}{1+bp} \qquad (15)$$

where c_h' is the saturation concentration [23]. b is the inverse of gas pressure p when the concentration is half of the saturation concentration. Concentrations provided by the dual sorption theory are considered the sum of both Henry and Langmuir sorption mechanisms.

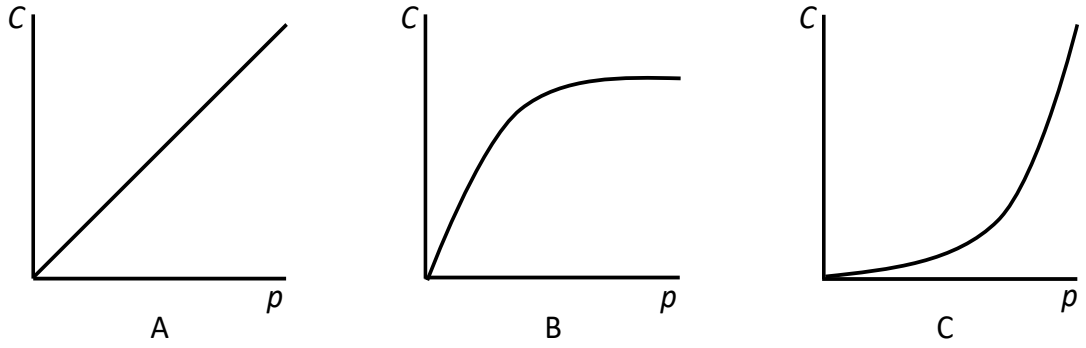

Figure 7. Isothermal sorption curves for Henry's Law sorption (A), Langmuir sorption (B) and Flory-Huggins sorption (C)

For non-ideal systems, strong interactions between the permeating substance and polymer are present. For such systems the absorbed gas concentration will tend to increase exponentially with increasing vapor pressure, as presented in figure 7C. This non-ideal sorption behavior is often described by free volume models and Flory-Huggins

thermodynamics [18]. The sorption behavior is related to plasticization of the polymer and cluster formations of the gas in present of strong solvent-solvent interactions.

In case of highly hydrophilic polymers, dissolution may occur through the combination of Langmuir sorption and Flory-Huggins interactions. The resulting sorption mode is often referred to as BET-mode [19]. At low water concentrations, polar groups on the polymer chains become strongly solvated by the gas. Within higher water activity regions, the concentration increase is dominated by clustering of water molecules and Flory Huggins interactions. Above a certain threshold, however, water clusters might become highly immobile and tend to deviate from participation in further diffusion.

2.11. Permeability of Polymers

Permeability is a result of dissolution of a penetrant onto a sample surface, followed by diffusion through it (under the influence of a concentration gradient), and subsequent desorption on the other side of the sample sheet. The permeation of molecules through a dense polymer relates the kinetic and thermodynamic contribution to mass transport phenomena:

$$Permeability\ (P) = \ Solubility\ (S) * Diffusivity(D) \quad (14)$$

when assuming ideal behavior and concentration independent transport coefficients. [18] Permeability is considered an activated process and can usually be described by an Arrhenius type of equation. The latter reveals the high temperature-dependency of the transport coefficients [18].

2.12. Relative Humidity

Relative humidity, water activity and vapor pressure are commonly used interchangeably. Relative humidity, RH, and water activity, a_w is given as the ratio of the partial pressure of vapor (p_w) within air at given temperature, to the equilibrium vapor pressure of water ($p_{w\ saturated}$) at the same temperature. This can be seen through:

$$RH\ (\%) = a_w * 100 = \frac{p_w}{p_{w\ saturated}} * 100 \qquad (15)$$

At 30 ℃, the equilibrium vapor pressure of water is 4.242 kPa [21]. The relation between the partial pressure of water vapor and relative humidity at 30 ℃ can be seen in figure 8 with water vapor pressures given in table 1.

Table 1. Water vapor pressures as a function of relative humidity at 30℃

RH [%]	p_w [Pa]	*RH* [%]	p_w [Pa]
14	594	*58*	2460
25	1061	*69*	2927
36	1527	*80*	3394
47	1994	*100*	4242

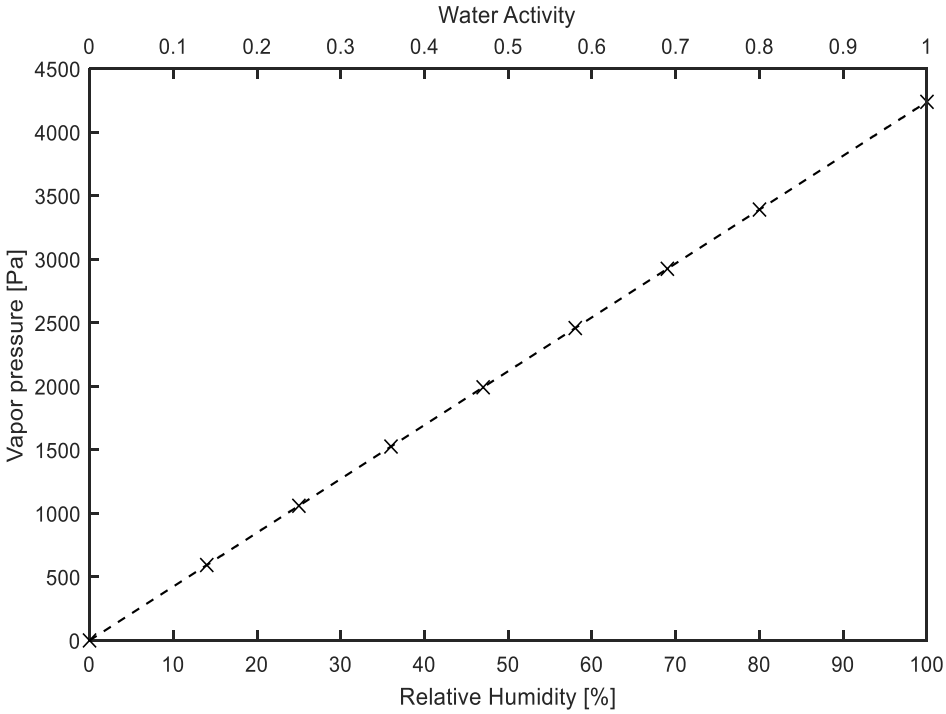

Figure 8. Relation between relative humidity, water activity and vapor pressure at 30℃ based on values presented in table 1

When assuming the vapor behaves ideally, and that the specific volume of the liquid is small compared to the specific volume of the vapor phase, the saturated vapor pressure can be found through integration of the Clausius-Clapeyron equation [22]. The solution to the equation gives the following expression:

$$p_2 = p_1 e^{\frac{-\Delta H_{vap}}{R}\left(\frac{1}{T_1}-\frac{1}{T_2}\right)} \qquad (16)$$

which relates the saturation pressure p_2 at a given temperature T_2 to a known saturation pressure p_1 at temperature T_1. The heat of vaporization (ΔH_{vap}) is the amount of energy required for the phase transition from liquid to gas and R is the specific gas constant. It is assumed that the heat of vaporization is unaffected by temperature.

2.13. Electric Resistivity

When a conductive swelling tape is exposed to an electric potential caused by the voltage differences across it, the resistance *R* of the tape determines the electric current flowing through it. This relation is specified through Ohm's law:

$$U = RI \qquad (17)$$

For objects behaving like ideal resistors this equation is valid, and a linear relation can be seen between the voltage *U* and the current *I*.

While the resistance is geometry dependent, the resistivity ρ is a material property. When a uniform current is transmitted through a uniform sample cross section of area *A* over the distance *l*, the resistivity can be determined from the object resistance and sample geometry through:

$$\rho = R\frac{A}{l} = \frac{1}{\sigma} \qquad (18)$$

[8] given in Ωcm. The conductivity σ of an object is defined by the reciprocal of resistivity and describes the materials ability for current to flow. The distance will be commonly referred to as the sample thickness.

2.14. Influence of Carbon Black

An inexpensive improvement in electrical conductivity of textiles is often provided by dip-coating in carbon black [23]. Carbon blacks are commonly formed by furnace processes and decomposition of oil. They consist of several spherical carbon-based nanoparticles combined into aggregates, with large specific surface area containing hydrophilic functional groups. The presence of hydrophilic groups causes energetic and entropic interactions upon mixing and increases the solubility of water in swelling tapes through hydration. However, strong hydrogen bonds cause immobile water molecules and they are restricted from participating in further diffusion. Alterations in functionality is provided by surfactants [24].

High conductivity is achieved by the presence of delocalized electrons e.g. charge carriers throughout the CB aggregates. This makes graphitization and material purity important features of conductive carbon blacks. The conductivity increase provided by CB coatings is a result of CB concentration [25]. A sharp increase in conductivity occurs when passing a certain concentration or percolation threshold where efficient conductive CB channels are formed. When the material is mechanically stressed, through e.g tensile stresses or volume expansion, conductive channels may become disrupted. This may reduce the electric conductivity of the coatings.

2.15. Ionic Conductivity

The conductivity of CB coated polyesters is governed by electronic charge carriers provided by functional carbon blacks. However, ionic SAPs or hydrogels may contribute to conductivity through ions. The presence of ionic charges causes partly neutralized polyacrylates to act as electrolytes upon swelling [9]. Spaced charges along backbone chains and their counterions may contribute to conductive paths [26], increasing the conductivity of swelling tapes. The resulting increase will be highly related to mobility of ionic substances.

2.16. Ageing in Polymers

In XLPE insulated HV cables, operational temperatures can be up to 90 ℃. The elevated temperatures are results of power losses within the conductor, which heats up surrounding component [6]. High temperatures over time can cause so-called ageing of polymers. Ageing

most often concerns deterioration of properties under influence of temperature, electric and mechanical stress and/or chemical reactions. If swelling tapes become affected by ageing, one potential effect is that water can migrate more easily to the insulation and reduce the lifetime of the cable.

Thermal degradation in polymers refers to chemical and physical processes occurring in polymers at elevated temperatures such as oxidation, chemical attacks and creeping. At elevated temperatures, these processes are accelerated. Thermo-oxidative reactions are considered the most important contribution to thermal degradation, inducing chain cleavage and depolymerization of chains and network structure. The process is governed by thermal initiation of free radicals and their reaction with oxygen to form peroxide radicals. This accelerates the degradation through subsequent propagation reactions [21]. Tertiary carbons are highly susceptible to radical stabilization and are common sites for degradation initiation.

In the presence of moisture, chemical ageing and material degradation may occur through hydrolysis. The process involves chemical reaction with water and subsequent polymer chain cleavage. Esters, ethers and amide bonds are particularly susceptible. The manufacturing of super-absorbents involves a variety of crosslinking agents e.g. TMPTA and diethylene glycol diacrylate, both of which contain ester bonds. Breaking of crosslinks through hydrolysis is commonly applied in the study of molecular weight distribution of the backbone polymer chains [9]. However, for swelling agents present within power cables, hydrolysis is highly unwanted as degradation of crosslinks results in reduced swelling capability, as can be seen in eq. 1.

Thermo-oxidation rates and hydrolysis are commonly described by the Arrhenius relation, given in eq. 19:

$$K(T) = Ae^{-\frac{E_A}{RT}} \qquad (19)$$

where the reaction rate K is given as a function of temperature T. R and A are the gas constant and frequency factor, respectively, while E_A is the activation energy of the reaction. The equation allows for lifetime assessment of polymers, and predictions on the combined effect of temperature and time. It has proven highly useful in accelerated testing and cab be used in the prediction of long-term exposure to elevated temperatures [27].

3. Experimental Methodology

3.1. Transport Coefficients Determination

Gravimetrical water uptake measurements were performed to characterize the mass transport properties of water vapor in a swelling tape. The presence of ionic-dipole interaction in SAP particles was assumed to be dominating the transport coefficients of the tape, providing non-ideal sorption and concentration dependant diffusion. By exposing the tape to a stepwise humidity increase of 11 % RH, the concentration dependency over each step was possibly reduced. This allowed for assumtions of a constant diffusion coefficient within the steps and for the theory to be be applicable. An illustration of the stepwise procedure can be seen in figure 9, with theoretical humidity and mass increase over time.

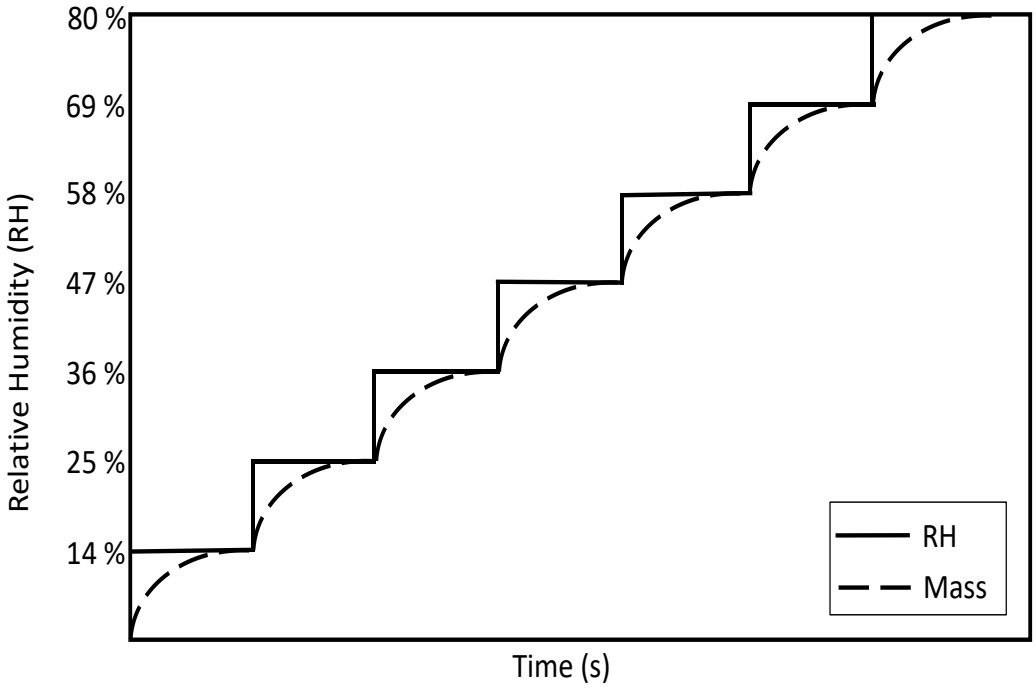

Figure 9. Theoretical mass increase of the sample (dotted line) when exposed to stepwise humidity increase (straight line)

3.1.1. Experimental Setup – Transport Coefficients

The mass increase was recorded by an ultra-microbalance of the Mettler Toledo UMX2 type, externally controlled through a LabView program. The program provided time settings for measurement initiation and mass recordings and a plot of the developing mass change with time. The balance was placed beneath a vertically adjustable dome, which could be controlled externally. The entire setup was placed in a climate chamber for temperature and humidity control. SIMPATI* software was used for external control of the chamber, using a customized test programme for each humidity step. Humidity sensors both inside and outside the dome were used to monitor the climate around the samples. The humidity sensors were of the type SENSIRON SHT75 COMSens. The setup for water uptake measurements can be seen in figure 10.

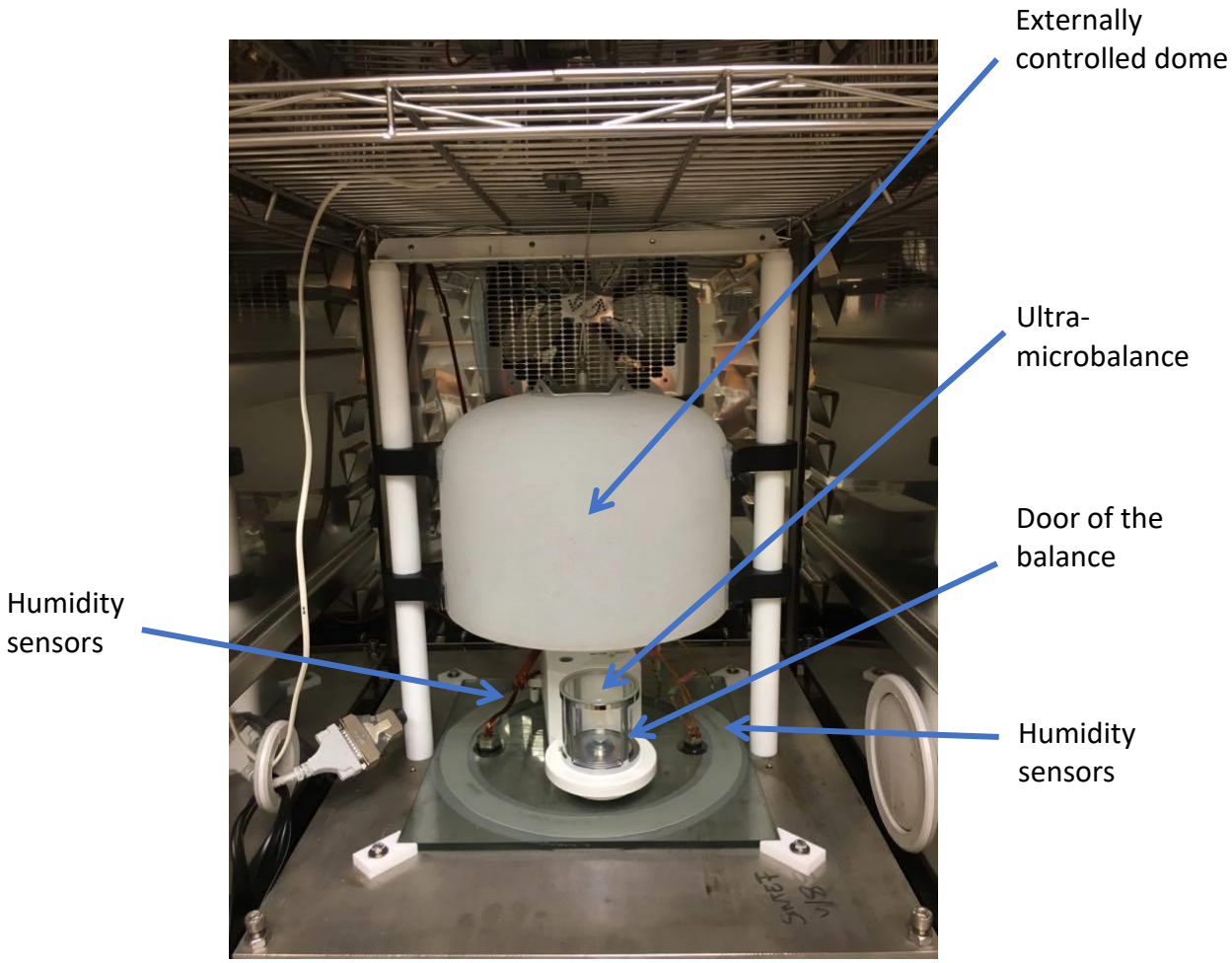

Figure 10. Setup for transport coefficients determination. The entire setup is placed within a climate chamber

3.1.2. Sample Preparation – Transport Coefficients

A swelling tape was cut into 36 discs of 2.5 cm diameter and 0.032 cm thickness[1] and separated on supporting needles. This was done to provide accessible sample surfaces during drying and equal initial surface concentrations during the water absorption measurements. A total of six samples were made, each containing six discs of tape, as seen in figure 11. The samples were placed in a vacuum chamber and dried for at least 14 days until the dry weight had stabilized. To prevent degradation or deterioration of the polymer structure the drying temperature was set to 30 ℃. Drying and its method is elaborated in appendix A.

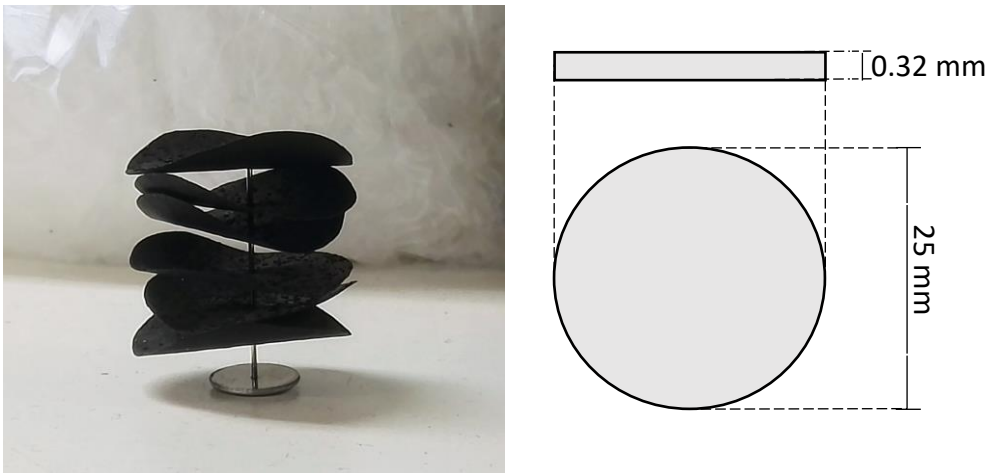

Figure 11. A sample consisting of six discs separated on a needle (right) and a schematic representation of the discs (left)

3.1.3. Experimental Procedure – Transport Coefficients

Due to vibrations affecting the balance stability, the climate chamber was turned off during the actual mass measurements. This was done by creating loops within the customized test programme which was synchronized with the recording LabView programme. A schematic representation of the loop and the measurement procedure can be seen in figure 12. Because of the assumptions made regarding concentration-dependent diffusion rates (see section 2.9) two separate measuring series were created. The series' loop-time were 3 and 5 minutes,

[1] The thickness of the tape at 50 % RH provided by the manufacturers datasheet

respectively. This was done to get sufficient sorption data for fast and slow occurring diffusion. The duration the loops were based on experiments done on a similar swelling tape in previous work [28].

After drying, a sample was placed in the climate chamber at 14 % RH and 30 ℃. The programmes controlling the balance and chamber were started immediately after this. The total time from turning off the vacuum to placing the sample within the chamber was 3 minutes, while the first measurement was taken after approximately 4 minutes. After a total of 30 seconds the chamber was turned on again and a new measurement loop was performed. The loops continued until the mass of the sample had stabilized and equilibrium was reached at a given vapour pressure. The temperature remained 30 ℃ during the entire measurement procedure.

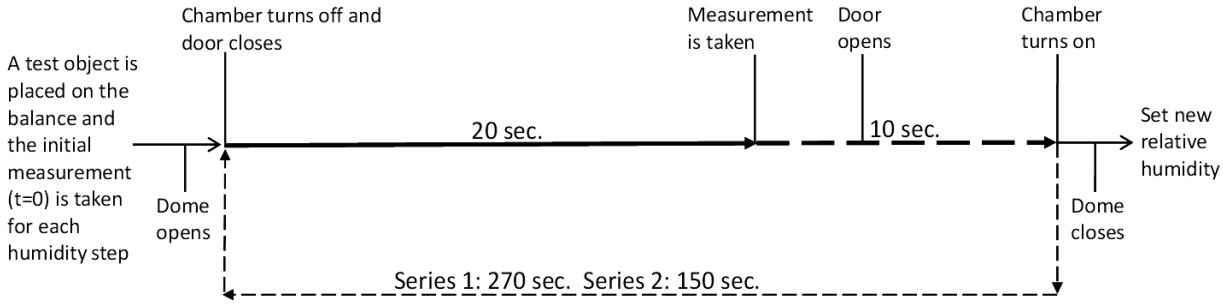

Figure 12. Schematic representation of the water sorption measuring procedure and synchronization. The loop timeline is given for the two separate measurements series

3.2. Resistivity of Humid Swelling Tape under Load

The resistivity of the swelling tape under load at various vapor pressures was measured to characterize the electric response of the tape at relevant humid conditions and compressions. Due to the anisotropic composition of the tape; implying inhomogeneous resistivity in two directions, the resistivity measurements were performed across (radial) and along with (axial) the tape. The directions are indicated in figure 13. Based on the two types of measurements, both the individual and synergistic effects of swelling and compression could be better understood in relation to the electrical properties of the tape.

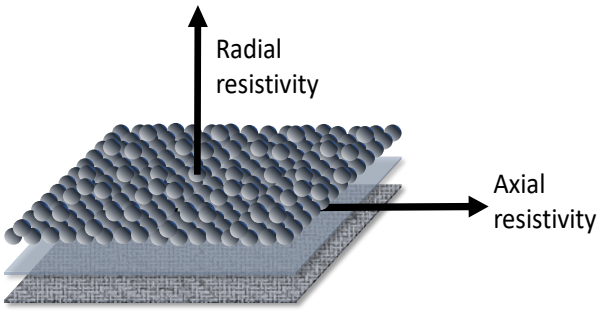

Figure 13. Radial and axial directions of the tape. The radial measurements were performed across the tape whereas the axial measurements were performed along with the tape

3.2.1. Experimental Setup – Resistivity Measurements

The resistivity measurements of the tape were performed in custom made four-terminal testing cells, commonly used for flat samples with low resistivity. A schematic representation of the cell used for radial measurements can be seen in figure 14. Figure 15 represents the cell used for axial resistivity measurements.

Both cells were composed of inner and outer electrodes, connected to a Keithley 2182A NanovoltMeter and a Keithley 2400 SourceMeter, respectively. By using a high-resistance voltmeter and keeping the electrodes insulated from each other it was possible to neglect wire and contact resistances in the circuit. Thus, the setups provided voltage measurements over the sample only, which is crucial when dealing with low resistance materials. The two meters were controlled through a LabView programme, where the current and measurement duration could be adjusted. The programme was designed to immediately plot the resulting voltage as a function of time in a graph, making it possible to evaluate the measurements while running. The measured voltage was the voltage needed to keep the current at given value.

The inner (sensing) and outer (sourcing) electrodes were physically divided into an upper part which could be lifted vertically for sample placement, and a stationary lower part. Equal potential between the upper and lower electrode pairs in the axial cell was provided through connecting wires. The design of the cell is based on the ISO 3915 standard for low resistance measurements of plastics made conductive by incorporation of carbon black.

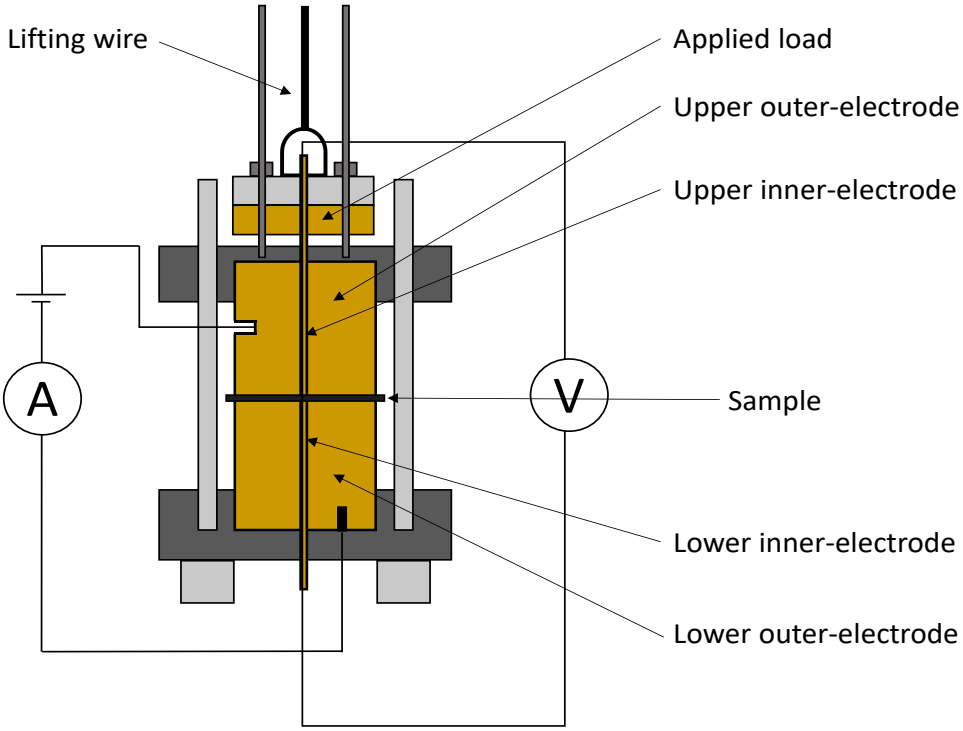

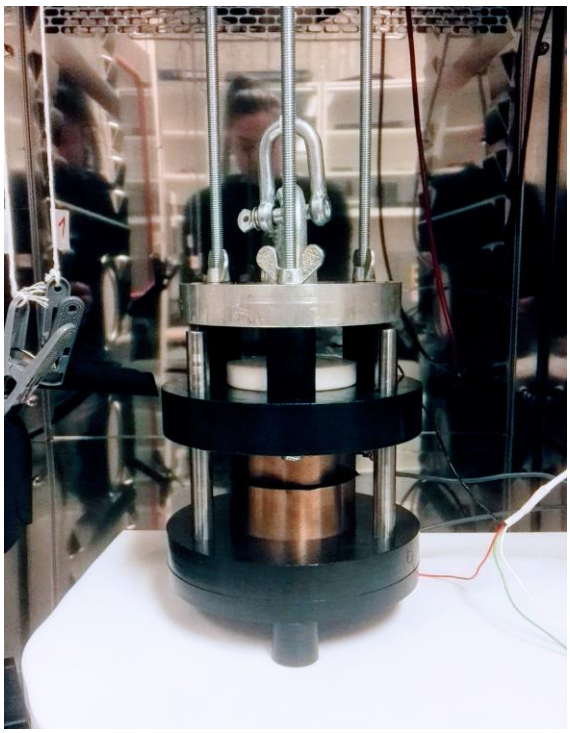

Figure 14. A schematic representation of the cross-section of the four-terminal testing cell used for measuring radial resistivity (top) and an image of the same cell (bottom)

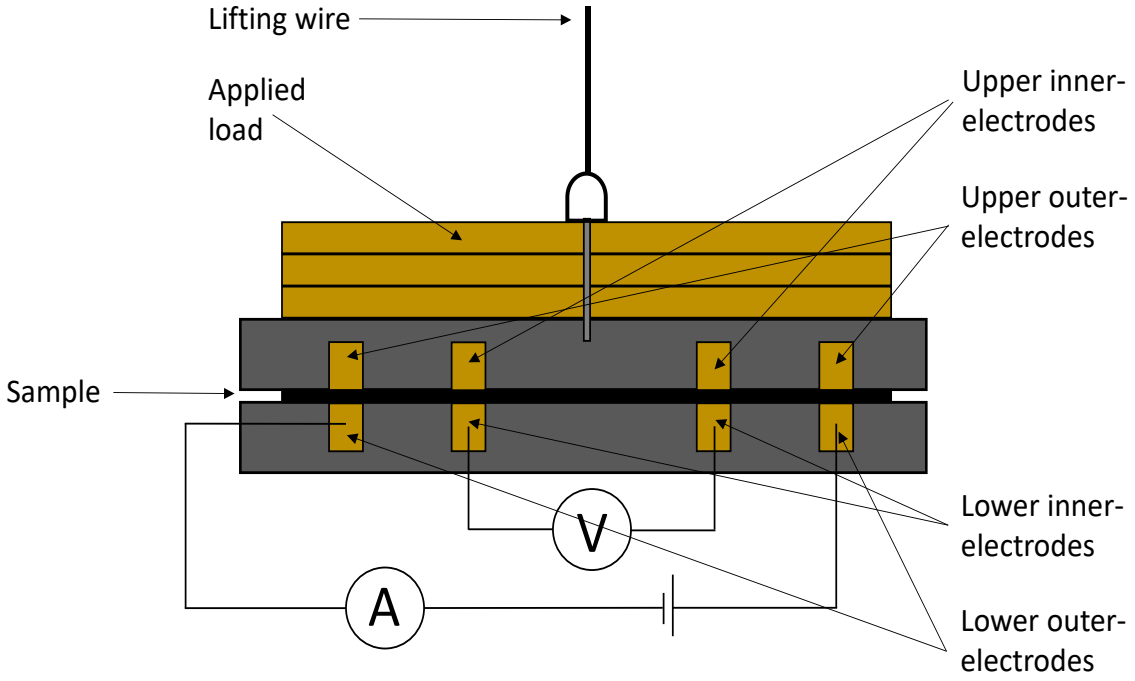

Figure 15. Schematic representation of the cross-section of the four-terminal measuring cell used for measurements of axial resistivity.

Loads were applied on the upper electrodes. A total of five loads were provided for each of the cells, giving the mechanical compressions presented in table 2. For comparison, the loads were related to sample geometry, providing equal pressurization in both radial and axial measurements.

Table 2. Weight sets and corresponding mechanical compression including electrodes

Weight set no.	1	2	3	4	5
Total Mechanical Compression [kPa]	6	8	10	23	33

The cells were placed within a climate chamber for stable climate conditions during resistivity measurements. To reduce the possible impact of a humidity change when opening the chamber door, lifting of upper electrode and loads were done automatically from outside the chamber. Sample placement could then be done through a small hole in the chamber wall which was covered during the measurements. Validation of the cell functionalities was done on a CB filled, polymeric material of known, homogenous resistivity in both radial and axial directions.

3.2.2. Sample Preparation – Resistivity Measurements

Radial measurements: A swelling tape was cut into 10 discs of 6 cm in diameter to cover the source electrodes of the cell. A total of five samples were made, each composed of two discs of tape, with a combined thickness of 0.064 cm.[2] This was done to enhance similarities to industrial application of swelling tapes.

Axial measurements: A swelling tape was cut into rectangular strips of 2 cm width, 14.5 cm length, and a thickness of 0.032 cm.[3] A total of five strips were made, providing five samples for the axial resistivity measurements.

[2] The thickness of the tape at 50 % RH provided by the manufacturers datasheet
[3] The thickness of the tape at 50 % RH provided by the manufacturers datasheet

Several sample parallels were used to reduce the impact of uneven SAP particle distribution and size on the average resistivity.

3.2.3. Experimental Procedure – Resistivity Measurements

For each measurement setup, five samples were conditioned within the chamber at 30 ℃ and 20 % RH for three days, to provide equilibrium water concentrations at given vapor pressure. The conditioning period was based on the results from the water uptake measurements and resulting time to equilibrium at similar humidity. After conditioning, the first sample (sample 1) was placed centred in the cell for uniform load distribution. To avoid the possibility of mechanical deterioration of the tape, weight sets were applied in increasing order.

The required potential over the sample for a given applied current and testing condition was measured and registered. The initial measurements were performed at 20 % RH and weight set 1. The sample was removed, and a new sample was placed. This continued until four measurements were taken for each of the five samples, and provided a reconditioning time between the measurements of minimum 5 minutes. The procedure allowed for enhanced reproducibility, stable water concentrations and reduction of left-over charges, induced by the voltage application. The current was set to 0.1 mA for a duration of 60 and 30 seconds, for radial and axial measurements, respectively. The current was based on calculated leakage currents in similar power cables, provided by SINTEF Energy Research. Measurement durations were chosen to avoid initial polarization contributions to current, found in similar a swelling tape in previous unpublished work [28].

After a total of 20 measurements, weight set 2 was applied to the cell and new measurements were performed in the same manner, at 20 % RH. The change in weight sets required that the door of the climate chamber was opened and altered the humidity within the chamber. A new conditioning period at relevant humidity was therefore necessary. This conditioning period was minimum two hours. The measurements then continued until the resistivity of the samples had been determined for all five weight sets. The humidity within the climate chamber was then increased and new sets of measurements could then be performed in the same manner. Subsequent conditioning period at new humidity was three days.

The axial and radial resistivity of the samples under load was determined at 30 ℃ and vapor pressures of 848 Pa, 1697 Pa, 2545 Pa and 3394 Pa, respectively, corresponding to 20

%, 40 %, 60 % and 80 % RH (see section 2.12). Sample thickness at 50 % RH was used in all calculations. It must be emphasized that the loads were applied after conditioning of the samples and must not be confused with swelling under load (conditioning period was not altered by changes in SAP-particle shape).

3.3. Ageing of Swelling Tape

Degradation of crosslinks will most likely affect the swelling properties, particularly water retention and swelling capability. To understand the consequences of thermo-oxidation and hydrolysis by water at operational temperatures over time, randomized tests were performed. The testing involved radial resistivity measurements and swelling height of aged and unaged samples. Accelerated ageing was performed at elevated temperature (aged dry) and in a combined environment of elevated temperature and high water vapor pressure (aged wet). The different ageing conditions can be seen in table 3. The ageing rate was assumed to follow an Arrhenius type of equation, as per section 2.16 and eq. 19. The volume of water was determined from vapor saturation concentrations at 110 ℃ according to eq. 16 and it was assumed that some vapor would leave the pressure cooker during the ageing period. The amount of oxygen is given by air density at 15 ℃, assuming 21 % oxygen in air.

Table 3. Parameters for ageing measurements

Ageing Condition	Temperature (℃)	Water (mL)	Oxygen (g)
Aged wet	110	250	~1.5
Aged dry	110	-	1.5
Unaged	-	-	-

3.3.1. Experimental Setup – Influence of Ageing

Radial Resistivity: The setup for radial measurements was the setup used for determining radial resistivity in section 3.2.1.

Swelling Height: Swelling height was measured by the commonly known “cup and piston“ method used for height measurements of swelling tapes. The apparatus consisted of a cup and a perforated, free moving piston. The inner diameter of the cup and the outer diameter of the piston were both 6 cm, respectively. An image of the apparatus can be seen in figure 16.

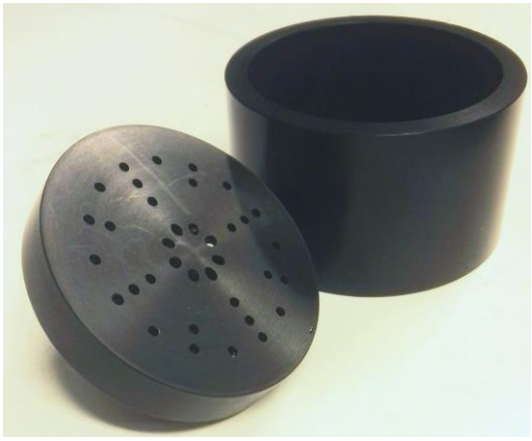

Figure 16. Cup and piston apparatus for swelling height measurements

3.3.2. Sample Preparation – Influence of Ageing

Radial Resistivity: Samples were prepared in the same manner as in section 3.2.2 - radial resistivity. A total of 15 samples were used, 5 for each ageing condition.

Swelling Height: 15 discs of 6 cm in diameter were cut from a swelling tape, giving 5 parallels for each ageing condition.

3.3.3. Experimental Procedure – Influence of Ageing

Ageing was performed in two 6 litre pressure cookers of type FUNKTION®, as seen in figure 17. The cookers allowed for total pressures of 1.9 bar and a maximum temperature of 120 ℃. 250 ml deionized water was added to one of the cookers, sufficient for saturated vapor conditions during ageing. Samples were placed on a perforated plate, held above the liquid water. Both cookers were placed in a heating chamber holding 110 ℃ and left for two weeks.

Aged and unaged samples were then dried for 72 hours and given random numbers for randomized tests.

Radial Resistivity: The resistivity was measured as in section 3.1.2 with weight set 1 and 5. The measurements were done at 20 % RH and 80 % RH, and two measurements were performed per sample.

Swelling Height: A sample was placed within the cup beneath the piston and initial height was measured. 10-15 ml distilled water holding 23 ℃ was poured onto the piston to completely fill the perforations throughout the entire measurement. Water absorption caused swelling of the tape and the height was measured as a function of time. The resulting height was measured every minute for a total of five minutes.

Figure 17. Samples placed in pressure cookers during ageing

4. Results and Discussion

4.1. Transport Coefficients of Water Vapor in a Swelling Tape

Diffusion and solubility coefficients are good tools for understanding the sorption properties of semi conductive swelling tapes. From the obtained water sorption data, diffusion and solubility coefficients were therefore determined. Due to instabilities within the climate chamber (particularly for measurements with 3 minute-loops and humidity below 47 % RH), average values of three samples were considered representative for the tape. Samples were chosen based on the stability of the chamber throughout the absorption measurements, through data provided by humidity sensors over each step. This is elaborated in section 4.1.1.1.

4.1.1. Diffusion Coefficients

From the sorption measurements, apparent diffusion coefficients were estimated through eq. 11, followed by model fittings of eq. 9 to experimental sorption data, assuming a constant diffusion coefficient within each step. For fitting of data concerning samples with initial concentrations $C_0 \neq 0$, the mass of water absorbed at previous steps was subtracted. The time before reaching equilibrium varied from more than three days (0-14 % RH) to around 30 minutes (58-69 % RH). This shows the complexity of the water absorption behaviour of the conducting swelling tape, and implies a significant dependency of water concentration on sorption and diffusion properties of SAP particles. A combined plot of the vapor sorption uptake over seven humidity steps can be seen in appendix B.

Figure 18 shows the sorption behaviour of vapor over the step 47-58 % RH for one sample with corresponding curve fitting. From the figure it is obvious that fittings were in good agreement with experimental sorption data, suggesting concentration independent diffusion. A fast, initial mass increase is observed which smoothly levels off at equilibrium concentrations. This is most likely to be caused by occupation of specific sites within the polymer structure and was the general case for steps above 36 % RH. This was also confirmed by analysing desorption, as seen in appendix C, which confirms the reversibility of this type of sorption. Based on the ease and rates of diffusion it can further be assumed that plasticization has occurred, according to section 2.9, and mobile chains are present.

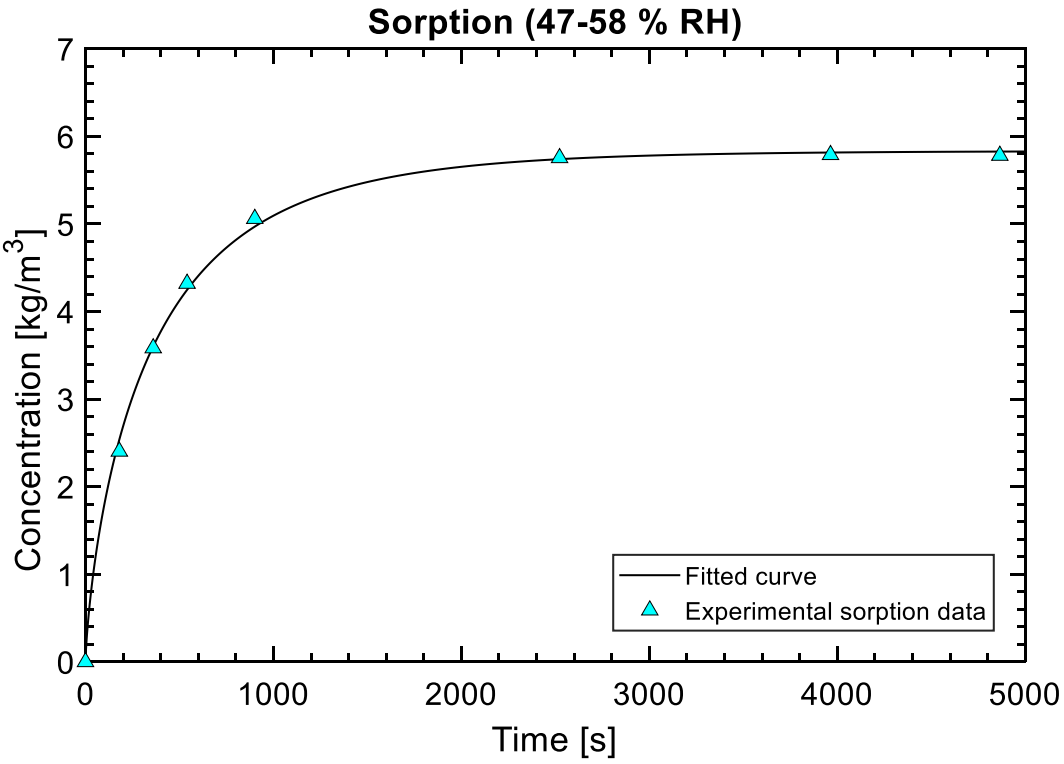

Figure 18. Experimental sorption data and fitting of eq. 9 over the step 47-58 % RH

At low water concentrations (<36 % RH), minor deviations from Fickian diffusion were observed, suggesting non-Fickian or anomalous diffusion. The sorption behaviour at 0-14 % RH can be seen in figure 19. From the figure, a two-step sorption was rather observed where rate of water vapor uptake was reduced at around 70 % saturation. The subsequent fitting provided higher diffusion coefficients and lower equilibrium concentrations over the concerning steps, compared to the experimental sorption data.

Sorption at low water concentrations can be explained by the dual-sorption mechanisms suggested in the theory (section 2.10), for polymers below their T_g. The kinetics are most likely to follow a sorption model where mobility of water depends on their interaction with the polymer matrix. This sorption mode postulates that there are two distinct populations of diffusing molecules occurring simultaneously; molecules are randomly dissolved in the matrix, following a Henry's Law sorption mode, whereas another population of molecules occupies specific sites according to Langmuir sorption. The two populations are

further considered to have distinct, constant diffusion coefficients [19] which correlates well with the sorption data presented in figure 19. Several authors have suggested mathematical expressions for estimation of an effective diffusion coefficient from dual-sorption kinetics [19, 29, 30]. However, this will not be performed in this report based on the fact that low water activities are highly unrealistic during operational conditions of the swelling tape, and that the offset from experimental data is only barely significant.

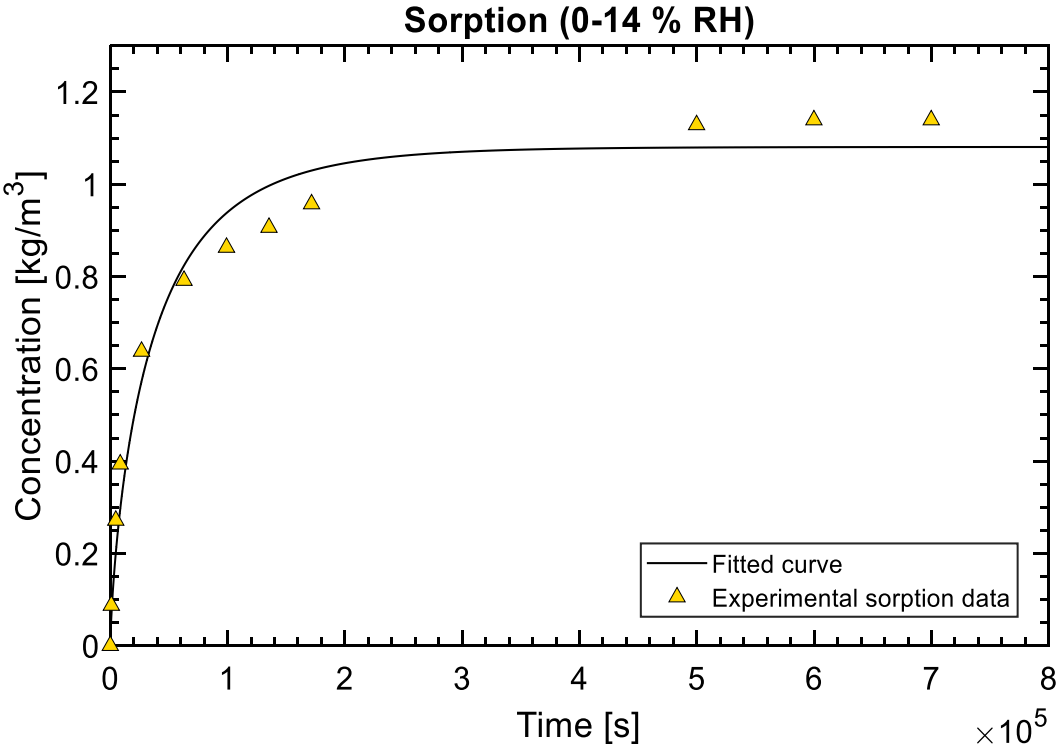

Figure 19. Experimental sorption data and fitting of eq. 9 over the step 0-14 % RH

Despite minor deviations, assumptions regarding Fickian diffusion were considered appropriate for all seven steps, and a constant diffusion coefficient was assumed. The resulting coefficients were plotted as a function of average water vapor pressure of each related step, as seen in figure 20. The markers represent average values of three samples with corresponding sample deviations. Apparent diffusion coefficients were added for comparison.

The diffusion coefficients were adjusted to a linear equation: $D = a_D p + b_D$ over several segments of water vapor pressures. Coefficients from the segmented linear regression are given in table 4.

Table 4. Diffusion coefficients as a function of vapor pressure over several segments

Vapor Pressure, p [Pa]	a_D	b_D
297-1294	2.64E-15	-6.61E-13
1294- 1760	2.93E-14	-3.50E-11
1760-2227	4.41E-15	8.82E-12
2227-2694	5.13E-14	-9.55E-11
2694-3160	-2.16E-14	1.01E-10

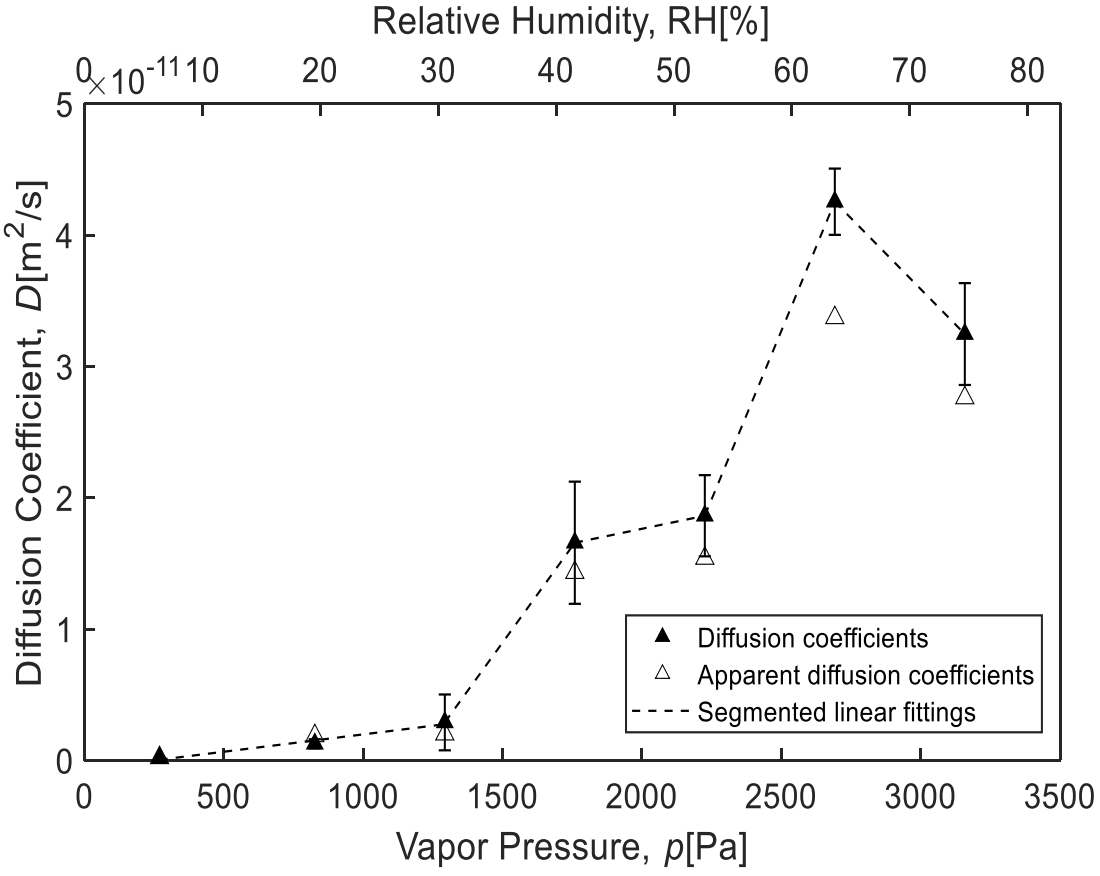

Figure 20. Diffusion coefficients as a function of vapor pressure

The figure gives a good indication of a concentration dependent diffusion rate over the entire humidity range. At low water activities diffusion of water molecules is significantly slow compared to rates at higher activities. This can be attributed low chain mobility, which is the rate limiting phenomena of diffusion according to the theory, and a consequence of glassy polymer states and reduced interaction volume. According to section 2.5, plasticization by moisture in hydrogels provide enhanced molecular mobility in the same manner as relaxation upon temperature increase. As water enters the structure, plasticization enhances mobility of the polymeric chains and ionic repulsions increases (see section 2.2) the volume for diffusion. A sharp increase in diffusivity is therefore observed. As a consequence, the coefficient increases from $1.6 \times 10^{-13} \frac{\mathrm{m}^2}{\mathrm{s}}$ at 7 % RH to $4.25 \times 10^{-11} \frac{\mathrm{m}^2}{\mathrm{s}}$ at 63.5 % RH.

The largest jumps in diffusivity is observed at the second and fourth step, where the coefficient increases by a factor of ten. This could possibly be attributed plasticization and an increase in the free volume through ionic repulsions, respectively. The maximum plateau is reached around 64 % RH. However, with further water content increase the diffusion coefficient slightly drops. This phenomenon has previously been observed by authors studying diffusion in hydrogels [31]. The slight drop in diffusion at high concentrations has been suggested to be a consequence of enhanced cluster formation caused by a predominance of solvent-solvent interactions and Flory Huggins sorption. At a certain point, large water clusters becomes immobile, and water molecules contained in them are prevented from contributing to diffusivity [31].

4.1.1.1. Sources of Uncertainties – Diffusion Coefficients

At low water activities the 3-minute loop provided unstable humidity within the chamber. After 30 seconds of being turned off, the humidity slightly increased and subsequent 2.5 minutes of being on was insufficient time for the desired humidity to be reached. To reduce the impact of humidity changes, 5-minute loops were applied in measurements concerning low humidity. However, slight variations within the climate chamber was still present and is likely to cause deviations over the three measurements. The impact of humidity changes on water sorption is elaborated in appendix C. Deviations could additionally be attributed the inhomogeneity of the tape e.g. SAP particle size, SAP distribution and CB content.

It must be emphasized that a constant film thickness (0.32 mm at 50 % RH) was assumed throughout the entire measurement. According to eq. 8 this is most likely to cause

over- and underestimated diffusion coefficients at low and high humidity, respectively, and even greater differences in diffusion over the entire humidity range. The thickness change of a similar swelling tape has been studied in a previous article [32]. The largest thickness deviation from dry tape was provided by a linear thickness increase with vapor pressure, increasing the diffusion coefficient by factor of 1.2 at highest. This suggest that the diffusion coefficients provided in figure 23 would reach no more than $5.1\times 10^{-11}\ \frac{m^2}{s}$ at 64 % RH, and most likely lower, considering the thickness is given at 50 % RH, and not at dry state.

From fittings of eq. 9 to experimental sorption data, the diffusion coefficient is given as an arithmetic mean of the data points; all data points are equally weighted. However, the fit adjustment increases with data points. Thus, an increasing number of data points at e.g. the initial sorption period or equilibrium would slightly improve adjustments at initial or equilibrium states, respectively.

From sorption data the diffusion coefficients were assumed to be constant over the related humidity step. However, the calculated coefficients are given as a mean value of related humidity step and was plotted accordingly (as a function of average humidity of start and final humidity). A segmented linear increase in diffusion coefficients with water vapor pressure was therefore suggested. Though this might not be the case it might give a good indication of how the diffusion coefficients change with vapor pressure.

4.1.2. Solubility Coefficients

Diffusion rates are highly related to molecular mobility. However, mobility is affected by alterations in solubility and interactions between molecules. The solubility coefficient of vapor within the swelling tape was therefore determined. This was done through application of eq. 13, with saturation concentrations provided from the fitting of eq. 9 to experimental sorption data. According to the theory and section 2.10, the solubility is related to interactions at equilibrium states. The resulting solubility coefficients were therefore plotted as a function of final vapor pressure for each of the seven steps and fitted to the equation 20:
$S = a_S p^2 + b_S p + c_S$, which provided the best goodness of fit. This can be seen in figure 21. Corresponding solubility coefficients are presented in table 5.

Table 5. Solubility coefficients as a function of vapor pressure

Vapor Pressure, p [Pa]	a_S	b_S	c_S
594-3394	5.72E-10	-5.77E-7	0.00263

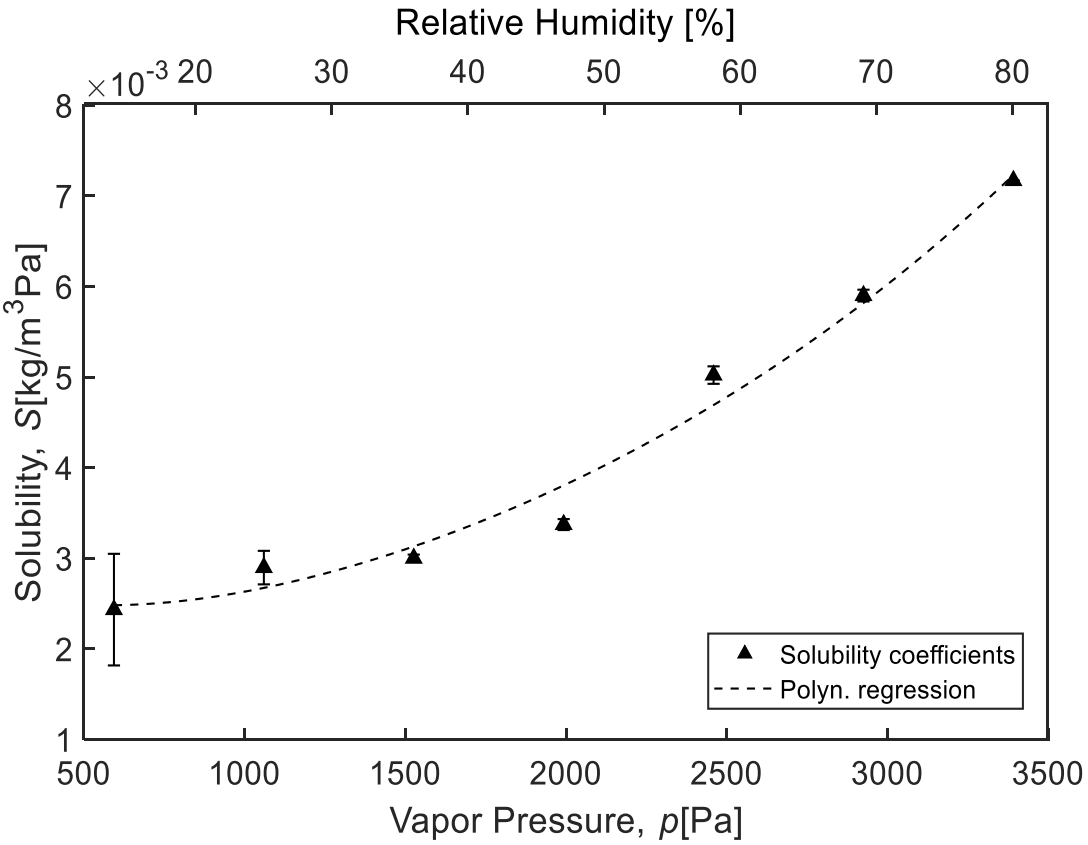

Figure 21. Solubility coefficients as a function of vapor pressure

From the plot, it is clear that the solubility of water within swelling tapes is concentration dependent. The increased sorption with water concentration is attributed the hygroscopic and polyelectrolyte property of the partly neutralized SAPs [31]. At initial low water concentrations, the solubility increases with increasing vapor pressure as water occupies specific sites within the polymer matrix. As water sorption continues, water is attracted through formation of strong ion-dipole interactions, and sodium ions lose their fixation to polymer chains. This results in volume expansion, possibly observed around 47 % RH.

Consequently, more water can be absorbed by the polymer structure [31]. Assumptions regarding volume increase seems to fit well with the increased diffusion rates observed previously.

The same phenomena has been suggested by another author [31]. The solubility can be considered being a result of three sorption mechanisms, where the Langmuir isotherm is saturated at lower water activity and Henrys sorption dominates. At higher concentrations the solubility increase is most likely to be attributed domination of Flory Huggins or solvent-solvent interactions and cluster formations of water [31]. A high degree of immobile water clustering is in good agreement with the decrease in diffusivity, as previously observed.

4.1.2.1. Sources of Uncertainties – Solubility Coefficients

Figure 21 shows larger deviations in solubility at the initial humidity step (0-14 % RH). The deviations are most likely to be attributed several factors. The initial concentration of water was assumed to be zero for all samples, however, the hygroscopicity of SAPs makes this highly unrealistic. With eq. 13 in mind, deviations in solubility over the initial step could be attributed alterations in initial presence of moisture, affecting diffusion rates and amount of water needed for reaching equilibrium conditions.

Exposure to various degrees of humid air between drying and the initial measurement could affect resulting equilibrium concentrations and hence the solubility coefficient, according to eq. 3 and eq. 13. The humidity during the exposure period varied between 10.3 % RH and 23.8 % RH for the samples, resulting in concentration increase of almost 0.0246 $\frac{kg}{m^3}$ and 0.15 $\frac{kg}{m^3}$, respectively. In the latter case, this resulted in a concentration increase of nearly 10 % of the equilibrium concentration at 14 % RH. The effect of exposure time and humidity is elaborated in appendix D.

The fact that samples were placed in the vacuum chamber at the same time (see section 3.1.2 and appendix A) altered the drying periods, possibly contributing to deviation in initial water concentrations. Also, SAP particle size could contribute to alterations in desorption period as diffusion rates decreases with increasing particle size.

In addition, it must be remembered that the swelling tape density at 50 % RH was used in determination of concentrations. According to eq. 9 and 13, this would promote lower solubility at low vapor pressures, whereas the solubility above 50 % RH would be slightly underestimated.

4.2. Radial Resistivity of the Swelling Tape

For CB-coated swelling tapes, the main contribution to conductivity is governed by presence of carbon black. However, radial resistivity concerns current flowing through an additional layer of SAP particles. To avoid enhanced current contribution from polarization phenomena (see appendix E), the average voltage over the last 30 seconds (of a total of 60 seconds) was calculated. From calculated voltage and application of eq. 17 and 18 and sample geometry, the resistivity of a swelling tape was determined. The distance over the sample (l) was set to 0.064 cm and the current was set to 0.1 mA throughout the entire measurements. The resistivity was determined at 20 %, 40 %, 60 % and 80 % RH. Application of Ohm's law was considered appropriate from the linear relation observed between the applied voltage and resulting currents. This can be seen in the appendix F.

To relate the humidity to water concentrations during resistivity measurements, equilibrium concentrations were plotted as a function of vapor pressure and fitted to an exponential equation. This can be seen in appendix G. The concentration as a function of water vapor pressure revealed similar trends as the solubility, with an exponential increase in water concentration with water vapor pressure. The relation between humidity during resistivity measurements, vapor pressure and water concentrations can be seen in table 6.

Table 6. Relations between relative humidity, vapor pressure and water concentrations in a swelling tape

Relative Humidity [%]	Vapor Pressure [Pa]	Water Concentration [kg/m^3]
20	848	1.9
40	1697	5.6
60	2545	12.5
80	3394	24.7

For average values to be representative it was important that the weight load did not affect the resistivity in a deteriorating manner; e.g. by preventing sufficient conditioning or destroying the polymer structure. The resistivity provided by each sample was therefore investigated by going through the resistivity data from the first to the fourth measurement. From the data, no correlations were found, regardless of sample, weight set and water concentration. This indicates an ability to withstand the applied load, provided by the crosslinked structure according to section 2.4, and that sufficient time (minimum 5 minutes) was provided for conditioning between measurements (see section 3.2.3). Average values were therefore considered appropriate for subsequent analysis.

The resistivity of a humid swelling tape was plotted as a function of mechanical compression, as seen in figure 22, with concentrations provided in table 5. The markers represent average resistivity of twenty measurements, using five different discs of swelling tape. Corresponding deviations are plotted as error bars.

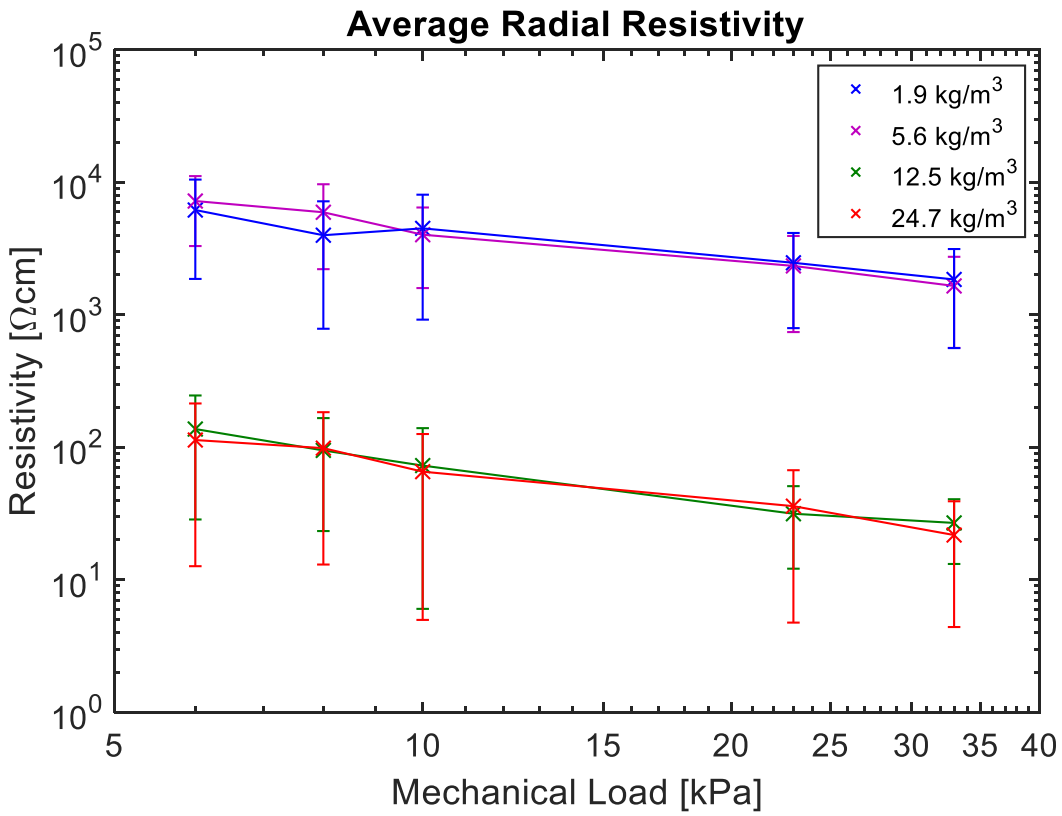

Figure 22. Radial resistivity as a function of mechanical load of a humid swelling tape containing four concentrations of water. The resistivity is given as an average of five samples with corresponding sample deviation

4.2.1. Effect of Humidity

By analyzing the effect of water concentrations in figure 23, a water-concentration dependent resistivity was observed. The increase in concentration from 1.9 $\frac{kg}{m^3}$ (20 % RH) to 5.6 $\frac{kg}{m^3}$ (40 % RH) showed no effect on resistivity. However, a significant reduction in resistivity was observed when the water concentration reached about 12.5 $\frac{kg}{m^3}$ (60 % RH). This resulted in average values dropping from around 5000 Ωcm to 50 Ωcm, a factor of 100. Above this concentration, no further alterations resistivity in were observed.

The resistivity drop at 60 % RH indicates a threshold were water alters the electric response of the swelling tape drastically. Several theories were therefore evaluated in order to explain this particular reduction. Water was assumed to contribute to resistivity decrease in three possible ways: an increase in sample thickness, reduced contact resistance and/or ionic contribution to conductivity.

Using a constant resistance of approximately 10 Ω (predicted from resistivity at 20 % RH/1.9 $\frac{kg}{m^3}$ and sample geometry at 50 % RH), the resistivity drop is assumed to be a result of thickness increase, using eq. 18. The thickness of the sample (l) would need to exceed over 5 cm, and more than 80 times its real height. To analyze thickness increase, swelling height measurements were performed (see section 4.3.1). The maximum swelling height in 15 ml deionized water holding 23 ℃ provided values of around 1.0 cm (two discs of tape) and no increase was detected when testing with water vapor. A previous article proposed a nearly linear increase in the projected area of SAP particles with increasing water concentration [32]. This is most likely to cause a linear thickness increase, assuming that volume expansion is linearly uniform in all directions. However, a linear resistivity decrease is in large disagreement with what is observed in figure 22. Thus, the resistivity decrease would need to be dominated by other factors. This was additionally confirmed by analyzing the resistance (does not consider sample geometry), as seen in figure E.1.

At 60 % humidity, the two discs composing a sample object became sticky and the sheets adhered to each other. Improved adhesion, in combination with the formation of soft, deformable SAP gels, could reduce the contact resistance and subsequent resistivity through an increase in electrical contact points.

From previous results, an increase in the interaction volume was possibly observed above 47 % RH. At this point sodium ions lose their fixation to polymer chains, and they become free to move within the structure. Also, carboxylate ions experiences enhanced

mobility upon plasticization. Improved ionic mobility, in combination with increasing amount of protons and lose sodium ions, could contribute a resistivity decrease through the formation of conductive ionic paths within the gel. A reduction in resistivity as a consequence of enhanced ionic mobility and increasing amount of ions, has previously been observed by authors studying conductivity within partly neutralized hydrogels [14, 26, 33]. It can thus be assumed that the reduced resistivity is a consequence of water-polymer interactions and increased amount of contact points, rather than subsequent increase in swelling height.

4.2.2. Effect of Compression

The effect of compression on the tape resistivity is small. From the error bars shown in figure 22, the resistivity of highly compressed tapes seems to provide values in the same range as lightly compressed tapes, regardless of humidity. However, a slightly decrease in resistivity with increasing compression was observed from average values.

When spherical SAP particles are compressed, they gradually transform into cylindrical discs. The degree of deformation is determined by the crosslink density and the resulting elastic modulus, which in turn is affected by humidity and plasticization (Also the rate of compression might affect deformation. However, the rate was equal for all samples and will not be further investigated in this report). As a result, the contact resistance is reduced, as previously mentioned. In addition, the total distance of transmitting current is reduced.

The fact that resistivity rather decreases with increasing mechanical compression also suggest that the effect of deswelling is minimal over the 1-minute of application of load. From the theory, compression would increase the chemical potential of water within the tape and cause water to diffuse to the surroundings. Consequently, the resistivity would increase according to figure 22. If a reduction in contact resistance and transmission distance reduces the resistivity of the tape, whereas deswelling increases subsequent resistivity, the effect of deswelling would seem to be minimal, considering that the resistivity is rather dropping.

4.2.3. Deviations from Average Values

From the figure, large deviations were observed. It must be remembered that between each measurement, samples were removed and replaced. By doing so, measurements were taken over different parts of two inhomogeneous tape sheets, which most likely contains uneven

SAP-particle distribution, SAP-particle size and CB content. As a consequence, the active area which is being measured is most likely change between each measurement and deviations would be observed. However, the largest deviations were attributed to particularly one sample. At low water concentrations and compressions, this sample provided significantly higher resistivities when compared to the other four. The impact of this sample can be seen when comparing figure 22 and figure H.1 in appendix H, the latter figure showing a large reduction in sample deviations. Microscopy at 20 % RH revealed alterations in sample topology of the concerning sample and a high SAP density was observed, which may explain the increased resistivity. Microscopy images and method can be seen in appendix I. Based on figure H.1, it could be assumed that the measuring method and apparatus provided good indications of the average tape resistivity and that the deviations were rather based on the inhomogeneity of the swelling tape.

4.3. Axial Resistivity of the Swelling Tape

In contrast to the radial resistivity of the tape, the axial resistivity of a swelling tape is assumed to dominated by the presence of conductive CB particles along the textile layer. For enhanced understanding of the anisotropic features of the tape, the axial resistivity was calculated. This was done by measuring the axial voltage over 30 seconds and subsequent calculations through eq. 17 and 18, and the corresponding sample geometry. Applied current was 0.1 mA. The values were plotted as a function of mechanical compression, as seen in figure 23, for samples containing four distinct concentrations of water. The correlations between humidity and water concentration can be seen in table 5.

Figure 23 shows resistivity values that are nearly unaffected by humidity and compression, suggesting that the electrical contribution of SAP particles to axial the resistivity is minimal. The values range between 16 and 20 Ωcm and little or no deviation was observed between the samples and the individual measurements. From the result, it can be assumed that an efficient layer of CB particles was present that the current is transmitted mainly through this layer. This was also confirmed through resistivity measurements and comparison of CB-filled poly(ethylene) sheet which provided similar resistivity.

A slight but significant increase in resistivity was observed when water concentrations increased to 24.7 $\frac{kg}{m^3}$. The increase in water concentration caused the resistivity to increase by a factor of 1.15, suggesting some distortion in CB distribution as water enters the tape. The

distortion could be a result of a slight volume expansion, as suggested in section 2.14, from swelling within hydrophilic polyester fibers composing the textile layers. However, due to the presence of highly crystalline fibrils, their interactions with water (see section 2.1) and subsequent swelling, is considered minimal, compared to swelling in SAPs. This could explain the reduced effect of humidity in the axial direction, compared to the radial direction.

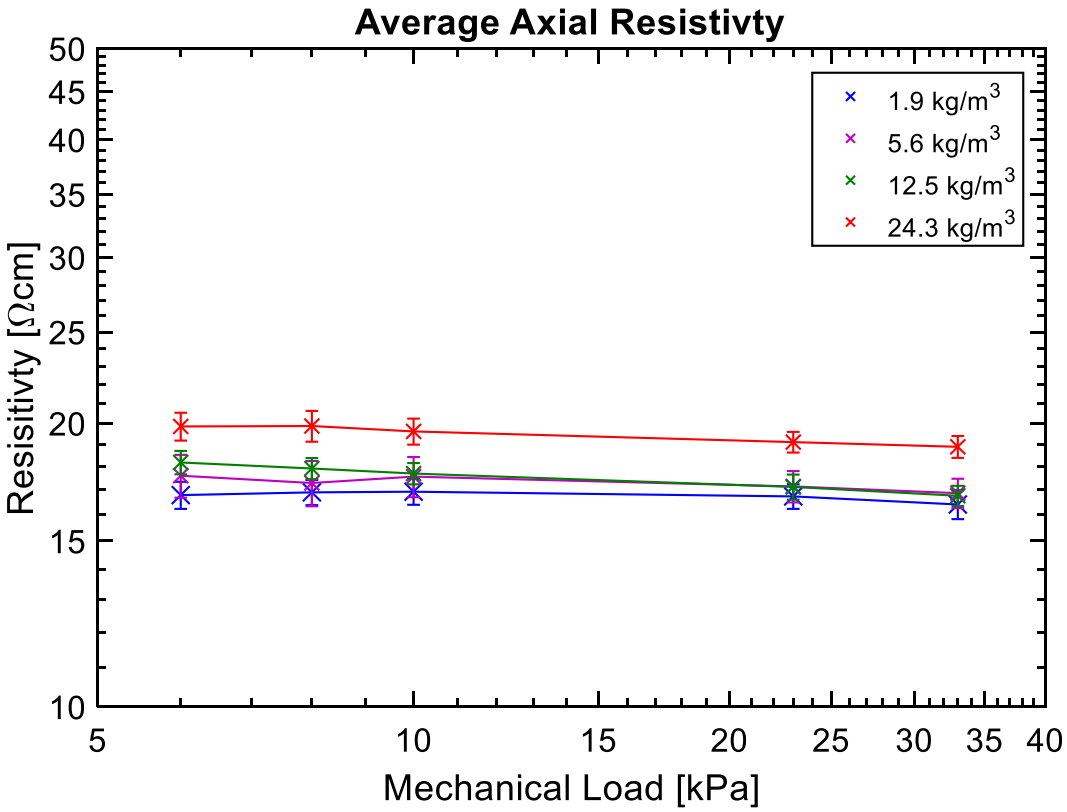

Figure 23. Axial resistivity as a function of mechanical load of a humid swelling tape containing four concentrations of water. The resistivity is given as an average of five samples with corresponding sample deviation.

At low water concentrations, average axial resistivity is more than 100 times lower than the radial resistivity of swelling tapes. However, as water concentration increased, the radial resistivity reaches values comparable to the axial values. The comparison between axial and radial resistivity of the swelling tape implies that efficient formation of CB channels also could be present in radial direction. The fact that the radial resistivity approaches axial resistivity with increasing humidity suggests that the impact of SAP particles on tape resistivity is lower at higher humidity.

4.4. Influence of Ageing

The properties of aged swelling tapes may deviate significantly from unaged tapes. The effect of ageing was therefore analyzed by randomized resistivity measurements and swelling height measurements. Both dry and wet ageing was performed to understand the impact of both thermo-oxidation and hydrolysis on moisture and water absorption. For simplicity, the randomized samples are presented with their ageing condition.

4.4.1. Radial Resistivity of Aged and Unaged Swelling Tape

The radial resistivity of aged and unaged samples was performed and compared to a reference. The resistivity was determined from current application of 60 seconds, where the last 30 seconds where considered steady state. The resistivity was determined from steady state values and application of eq. 17 and 18 and sample geometry. A total of two measurements were performed per sample. There was no decreasing or increasing trend in resistivity from the first to the second measurement, regardless of sample, humidity, weight set and ageing. Average resistivity of the two measurements was therefore used.

The resistivity of aged and unaged (reference) samples was plotted as a function of mechanical compression, measured at two water concentrations, as seen in figure 24. The figure shows insignificant effect of ageing on the resistivity, regardless of wet of dry ageing conditions. Not surprisingly, the ageing would seem to have no effect on CB particles and subsequent conductivity. As previously observed, the resistivity dropped when concentrations of water exceeded 12.5 kg/m^3. However, the extent of resistivity decrease with water concentration is slightly reduced after ageing.

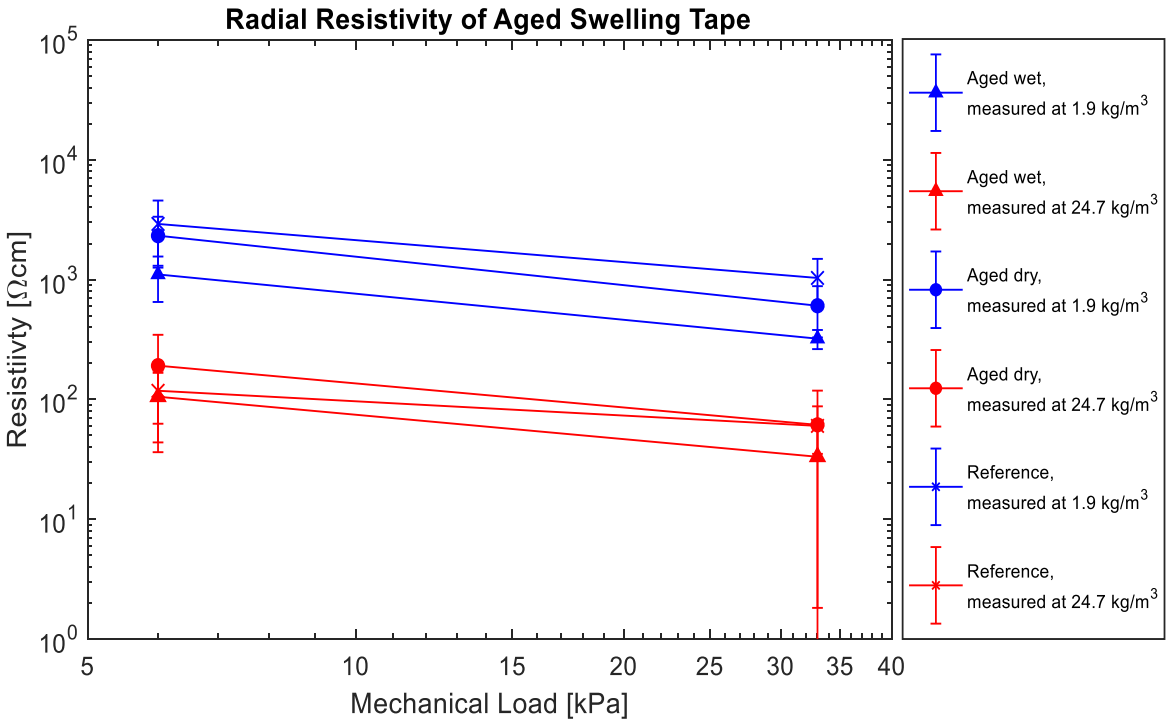

Figure 24. Radial resistivity as a function of mechanical compression of aged and unaged swelling tape, containing two concentrations of water (red and blue). The markers are given as an average of five samples with corresponding sample deviation. Two measurements were provided per sample

4.4.2. Swelling Height of Aged and Unaged Swelling Tape

Swelling height of aged and unaged tape was measured to understand the influence of ageing on swelling capability, when exposed to liquid water. The results from the randomized tests can be seen in figure 23, giving the height of 15 samples as a function of time. The values indicate a reduction in swelling height for the wet-aged samples, reaching about 0.08 cm. There was no significant distinction between dry-aged and reference samples. However, the reference samples provided the maximum swelling heights, ranging between 0.32 to 0.47 cm, whereas dry-aged tapes showed heights around 0.28 cm.

From the results it is obvious that ageing in combination of vapor and elevated temperature affected swelling heights to a large degree. The synergic and individual effects of hydrolysis and thermo-oxidation has possibly resulted in cleavage of crosslinks containing susceptible ester, ether and amide bonds. Chain cleavage and subsequent degradation of crosslinks can retard water retention capacity according to eq. 1 and lower the resulting swelling height.

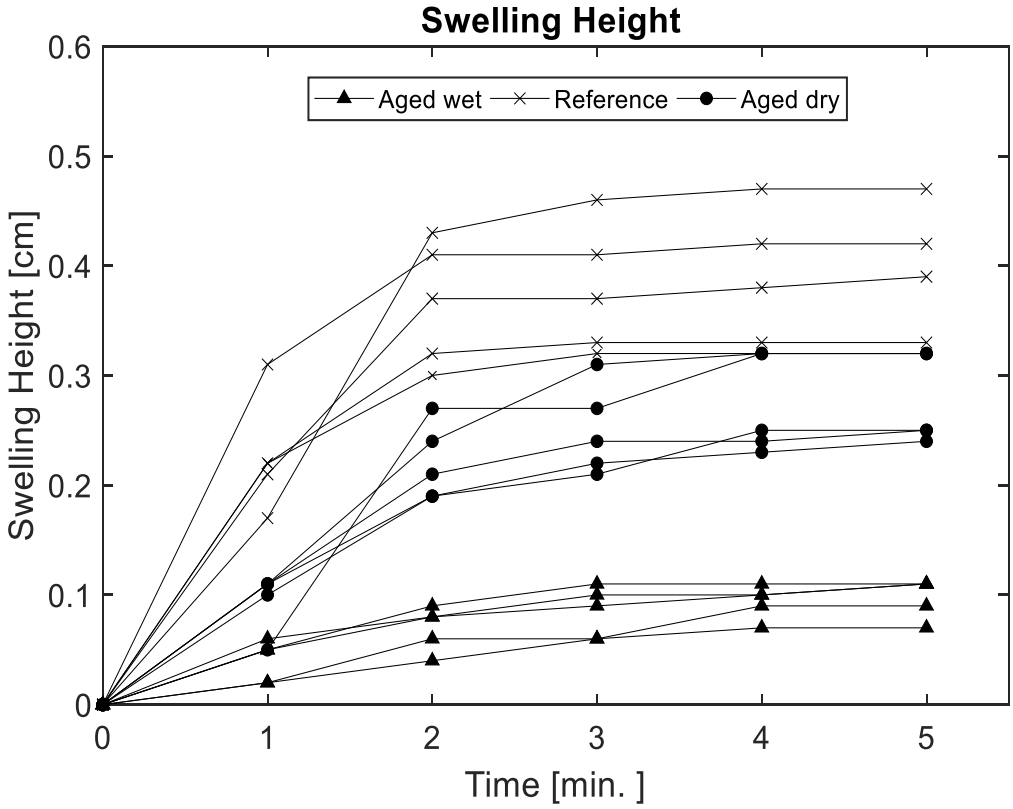

Figure 25. Swelling height as a function of time for aged and unaged samples

Based on the combined results of ageing, from resistivity and swelling height measurements, it could be assumed that ageing had minimal impact on water vapor absorption. This is most likely due to the low amount of water being held by the structure compared to fully swollen states. It must be remembered that the SAP particles are able to absorb more than 100 times their own weight through chain extension and subsequent volume increase. From previous sorption results it is obvious that the SAPs are far from reaching maximum swelling, and chain extension is scarcely present. Thus, the degradation of e.g.

crosslinks would not contribute to absorption by vapor to the same extent as absorption by liquid water. The effect of moisture on resistivity would consequently remain the same. The effect of ageing is, however, larger when analyzing swelling height. This can be attributed to a larger volume expansion caused by sorption of liquid water. The large volume expansion depends on crosslinks and chain extension to a larger degree than sorption by water vapor. The results from the swelling height measurements indicated that ageing occurred, and the method was considered appropriate.

5. Conclusions

5.1. Transport Coefficients

A successful method was applied in order to determine the diffusion coefficients of a semi conductive swelling tape in the range of 7-75 % RH. Within this range, the swelling tape possesses concentration dependent diffusion coefficients which increases non-linearly with water vapor concentration. The increase in diffusivity is most likely a result of enhanced plasticization by water vapor in combination with increasing free volume from ionic repulsions. A slight drop in diffusivity was observed at high humidity which could be attributed the formation of immobile water clusters. The diffusion coefficients ranged between $1.6 \times 10^{-13} \frac{\mathrm{m}^2}{\mathrm{s}}$ and $4.25 \times 10^{-11} \frac{\mathrm{m}^2}{\mathrm{s}}$.

The solubility of the tape increases non-linearly with water vapor pressure in the humidity range of 14-80 % RH. The solubility has been found to follow the equation: $S = 5.72 \times 10^{-10} p^2 - 5.77 \times 10^{-7} p + 0.00263$ within the given humidity range. The solubility can be assumed to follow several sorption modes which is most likely to be attributed to the hygroscopic and polyelectrolytic nature of the SAPs.

5.2. Electrical Resistivity

The electrical resistivity of the tape was determined in two directions. The radial resistivity of the tape showed a significant reduction in resistivity when water concentrations exceeded 5.6 $\frac{kg}{m^3}$. This resulted in a reduction in axial resistivity from around 5000 Ωcm to 50 Ωcm. The reduction in resistivity above a certain concentration threshold could be attributed to a decrease in contact resistance and increasing ionic contribution to conductivity.

The effect of compression on radial resistivity was insignificant. However, a decreasing trend in resistivity was observed with increasing compression, a possible consequence of increased contact points and reduced current transmission distance. The effect of compression on SAP deswelling was considered to be minimal.

The axial resistivity of the tape suggested that efficient CB paths were present in the axial direction, regardless of humidity and compression. The resistivity ranged between 16 and 20 Ωcm. A slight, but significant increase in axial resistivity was observed when water concentrations reached 24.7 $\frac{kg}{m^3}$, possibly due to slightly distortions in the CB channels.

At high water concentrations and mechanical compression, the radial resistivity of the tape approached axial resistivity. It could thus be assumed that efficient CB paths were present in both directions under these conditions. From both types of electrical measurements, it was concluded that the effect of SAPs on tape resistivity was reduced with increasing humidity.

5.3. Effect of Ageing

The effect of ageing on tape resistivity was minimal. However, a significant reduction in swelling height was observed for wet-aged samples. The measurements suggested that CBs were unaffected by ageing, and that sorption of liquid water was influenced by ageing to a larger degree than sorption by water vapor. The influence of ageing of swelling height was attributed a possible deterioration of the SAP structure.

References

1. Hussain, A.B., A. Matar, and T. Yasmin, *CO2 emmisions, energy consumption, economic growth, and financial development in GCC cuntries: Dynamic simultanoeus equation models.* Renewable and Susstainable Energy Reviews, 2017. **70**: p. 117-132.
2. York, R., *Demographic trends and ebnergy consumption in European Union Nations, 1960-2025.* Social Science Research, 2007. **36**(3): p. 855-872.
3. Best, R. and P.J. Burke, *The Importance of Government Effectiveness for Transitions toward Greater Electrification in Developing Countries.* Energies, 2017. **10**(9).
4. International Energy Agency *World Energy Outlook 2017*. 2017.
5. International Energy Agency, *WEO 2017 Special Report - Energy Access Outlook 2017*, OECD/IEA, Editor. 2017: France.
6. Worzyk, T., *Submarine Power Cables*, in *Design, Installation, Repair, Environmental Aspects*, Springer, Editor. 2009, Springer-Verlag Berlin Heidelberg. p. 296.
7. Radu, I., et al., *The danger of water trees in polymer insulated power cables evaluated from calculations of electric field in the presence of water trees of different shapes and permittivity distributions.* Journal of Electrostatics, 1997. **40**: p. 343-348.
8. Ildstad, E., *Insulating Materials for High Voltage Applications*, in *TET 4160*. 2017, NTNU: Trondheim.
9. Buchholz, F.L. and A.T. Graham, *Modern Superabsorbent Polymer Technology*. 1998, United States of America: John Wiley & Sons.
10. Brydson, J.A., *Plastic Materials*. 7 ed. 1999, Oxford: Butterworth-Heinemann. 920.
11. Krevelen, D.W.V., *Properties of Polymers*. 2009, Amsterdam: Elsevier.
12. Hill, R. and E.E. Walker, *Polymer Constituttion and Fiber Properites.* Journa of Polymer Science, 1948. **3**(5).
13. Wu, Y., S. Joseph, and N.R. Aluru, *Effect of Cross-Linking on the Diffusion of Water, Ions, and Small Molecules in Hydrogels.* Physical Chemistry, 2009. **113**.
14. Pissis, P., A. Kyritsis, and V.V. Shilov, *Molecular mobility and protonic conductivity in polymers: hydrogels and ionomers.* Solid State Ionics, 1999. **125**(1-4): p. 203-212.
15. Z.HPing, et al., *States of water in different hydrophilic polymers — DSC and FTIR studies.* Polymer, 2001. **42**(20): p. 8461-8467.
16. Crank, J., *The Mathematics of Diffusion*. Vol. Academic Press 1956, Oxford.
17. Crank, J. and G.S. Park, *Diffusion in Polymers*. 1968, Great Britain: Academic Press.
18. Mulder, M., *Basic Principles of Membrane Technology*. 2003, Dordrecht: Kluwer Academic Publishers.
19. Klopffer, M.H. and B. Flaconnèche, *Transport Properties of Gases in Polymers: Bibliographic Review.* Oil and gas Science Technology, 2001. **56**(3).
20. Chen, P., *Molecular Interfacial Phenomena of Polymers and Biopolymers*. 1st ed. 2005: Woodhead Publisher.
21. Zumdahl, S.S. *Chemical Principles*. 2005 [cited 2017; 5th:[
22. Velasco, S., F.L. Román, and J.A. White, *On the Clausius–Clapeyron Vapor Pressure Equation.* Journal of Chemical Education, 2009. **86**(1): p. 106-111.
23. Åkerfeldt, M., *Electrically Conductive Textile Coatings*, in *Faculty of Textiles, Engineering and Buissness*. 2015, University of Borås: Borås.
24. Schultz, J., E. Papirer, and C. Jaquemart, *Mechanisms of Diffusion of Water in Carbon Black Filled Polymers.* Eur. Polymer Journal, 1986. **22**(6): p. 499-503.

25. Negru, D., C.-T. Buda, and D. Avram, *Electrical Conductivity of Woven Fabrics Coated with Carbon Black Particles.* Fibers & Textiles in Eastern Europe, 2012. **20**(1): p. 4.
26. Li, H., et al., *Ionic Conductivity in Polyelectrolyte Hydrogels.* Macromolecules, 2016. **49**: p. 9239-9246.
27. Maxwell, A.S., et al., *Review of accelerated ageing methods and lifetime techniques for polymeric materials*. 2005: United Kingdom.
28. Olsen, M.N.P., *Characterization of a Non-Woven Swelling Tape*. 2017, NTNU: Trondheim.
29. X.J.Fanac, S.W.R.Leeb, and Q.Hanc, *Experimental investigations and model study of moisture behaviors in polymeric materials.* Microelectronics Reliability, 2009. **49**(8): p. 861-871.
30. Placette, M.D. and X. Fan, *A Dual Stage Model of Anomalous Moisture Diffusion and Desorption in Epoxy Mold Compounds*, in *Int. Conf. on Thermal, Mechanical and Multiphysics Simulation and Experiments in Microelectronics and Microsystems*. 2011, IEEE.
31. Chun, M.-S. and D.-Y. Lee, *Water Sorption and Hindered Diffusion with Different Chain Stiffness of Superabsorbent Polymer.* Bulletin of the Korean Chemical Society, 2015. **36**: p. 269-275.
32. Orvedal, I., *Måling og modellering av vanntransportegenskaper til svelleband til høyspenningskabler*, in *IFY*. 2011, NTNU: Trondheim.
33. Pissis, P. and A. Kyritsis, *Electrical conductivity studies in hydrogels.* Solid State Ionics, 1997. **97**(1-4): p. 105-113.
34. Patsch, R., J. Menzel, and D. Kamenka *Dielectric Time Constants - teh Key to Interpretation of Return Voltage Measurements on Cellulose-Oil Insulated Power Equipment*. 2010.

Appendix

A. Drying of Swelling Tapes

Drying of samples was performed in order to get initial dry weight for water uptake. measurements. Drying proceeded in a vacuum chamber at 30 ℃ and the resulting mass reduction was measured by a micro-balance of type Mettler Toledo UMX2. The dry weight was measured with 0.01 mg accuracy. To minimalize exposure time to air after removal from vacuum chamber the balance was placed in immediate access. The time between turning on the air pressure within the chamber and measurement was approximately 3 minutes. The mass was plotted as a function of time, as seen in figure A.1, and fitted to the curve $M = a_M e^{b_M t} + c_M e^{d_M t}$. The drying coefficients can be seen in table A.1. From figure A.1 a drying period of 14 days was considered appropriate. However, for samples experiencing larger drying periods it can be assumed that desorption would continue with drying time and eventually cause some deviations over the first humidity step.

The hygroscopicity and inhomogeneity of SAPs made drying of the swelling tape rather difficult. The 3-minute exposure to humid air is most likely to cause deviations in measured, however decreasing, dry weight. It was observed that samples with drying period of seven days at 30 ℃ experienced desorption of water when placed within the climate chamber holding 14 % RH. This suggested that water was still present within the tape after seven days of drying or that sorption of moisture occurred during exposure to humid air. The impact of exposure time and humidity is elaborated in appendix D. Also, inhomogeneous SAP particle/granulate size could have deviating impact on the dry weight through alterations in desorption rates.

Table A.1 Mass as a function of drying period

Time, t [days]	a_M	b_M	c_M	d_M
0-21	3.292	-0.3546	358.7	-1.425E-05

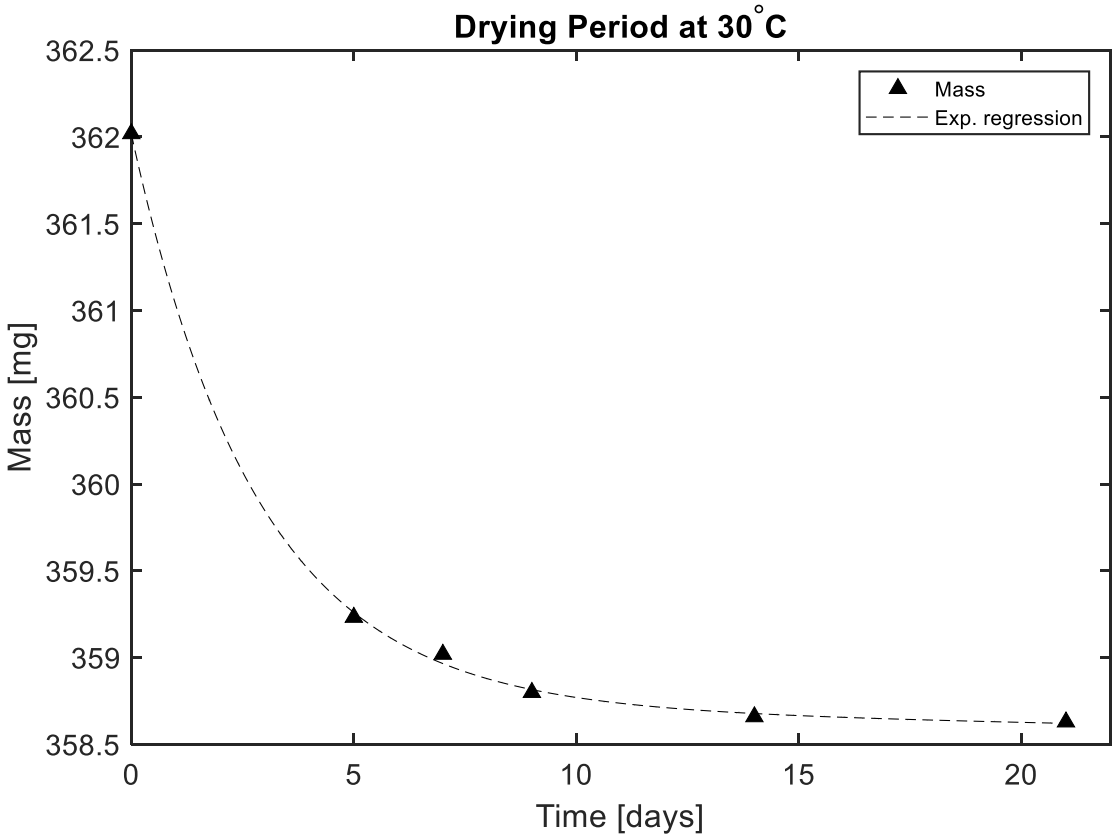

Figure A.1. Mass reduction at 30℃ as a function of time

B. Sorption Kinetics at 30 ℃

From experimental sorption data and curve fitting of eq. 9 the sorption kinetics over seven humidity steps could be analyzed. A combined plot be seen in figure B.1. The figure shows concentrations of absorbed water as a function of time, given initial conditions: $C_0 = 0$. From the figure, variations in water uptake was observed, ranging from around 1 $\frac{kg}{m^3}$ to 7 $\frac{kg}{m^3}$ at first and last step, respectively. Below 47 % RH, water uptake increased with increasing steps. However, a significant increase in water uptake occurred above 47 % RH which could indicate presence of larger interaction volume from ionic repulsions and more water can be retained within the structure. This correlates well with the large increase in diffusivity (time before reaching equilibrium) observed from the third to the fourth step. A large increase in diffusivity is also observed at the second step, suggesting plasticization and enhanced chain mobility.

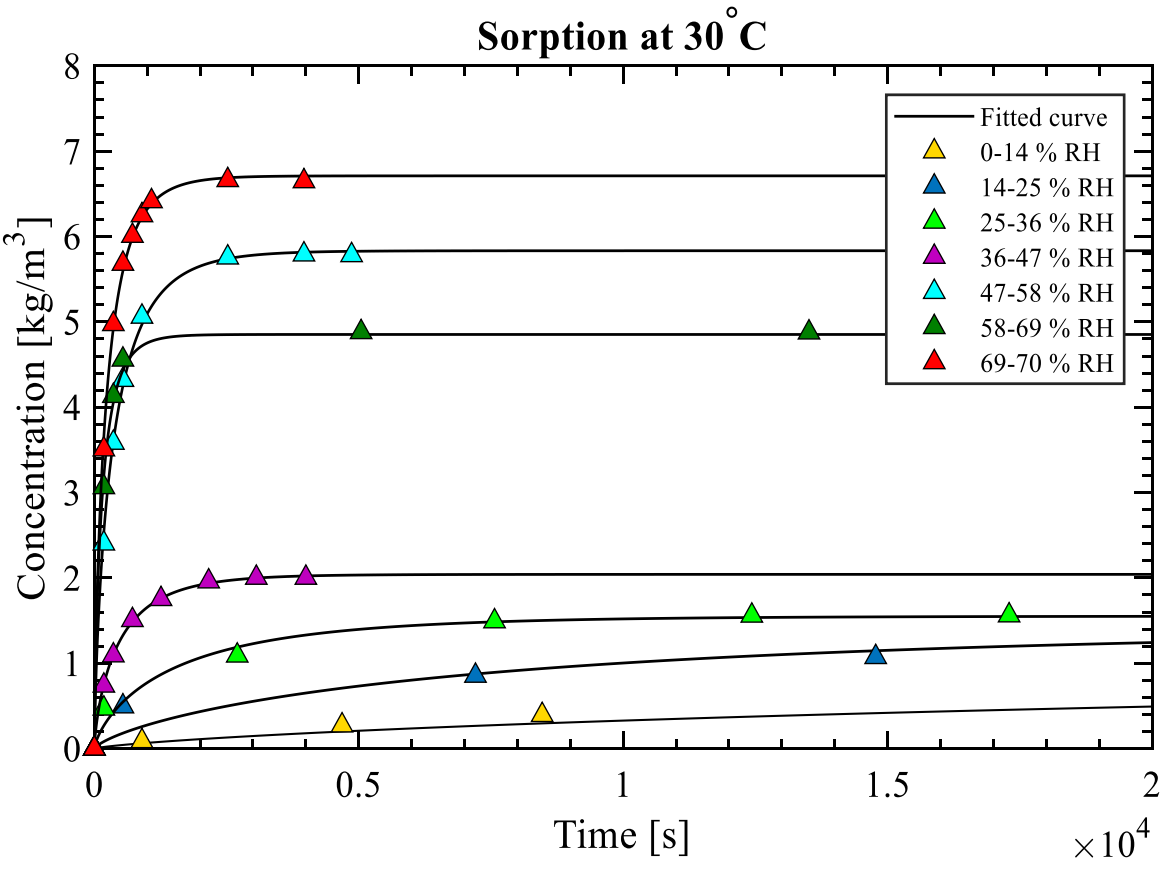

Figure B.1. Sorption at 30℃ over seven humidity steps

C. Absorption and Desorption with Changes in Humidity

From sorption measurements over the step 36-47 % RH the humidity within the chamber was increased to 50 % RH, after equilibrium at 47 % RH was reached. This can be seen in figure C.1 where the blue curve represents the humidity and the markers represent sorption data. A nearly instant absorption and desorption of vapor was observed which is considered being a consequence of a reversible process. This suggest that water was occupying specific sites in the polymer structure rather than being chemically bonded to the polymer chains. The high concentration dependency of slightly changes in humidity can explain some of the deviations observed in diffusion and solubility constants between the three samples.

At low water activity, however, sorption was assumed to be non-fickian, suggesting that chemical interactions between solvent and polymer are present. The resulting desorption at low humidity would most likely be a much slower, rather irreversible process and possibly not occurring at all.

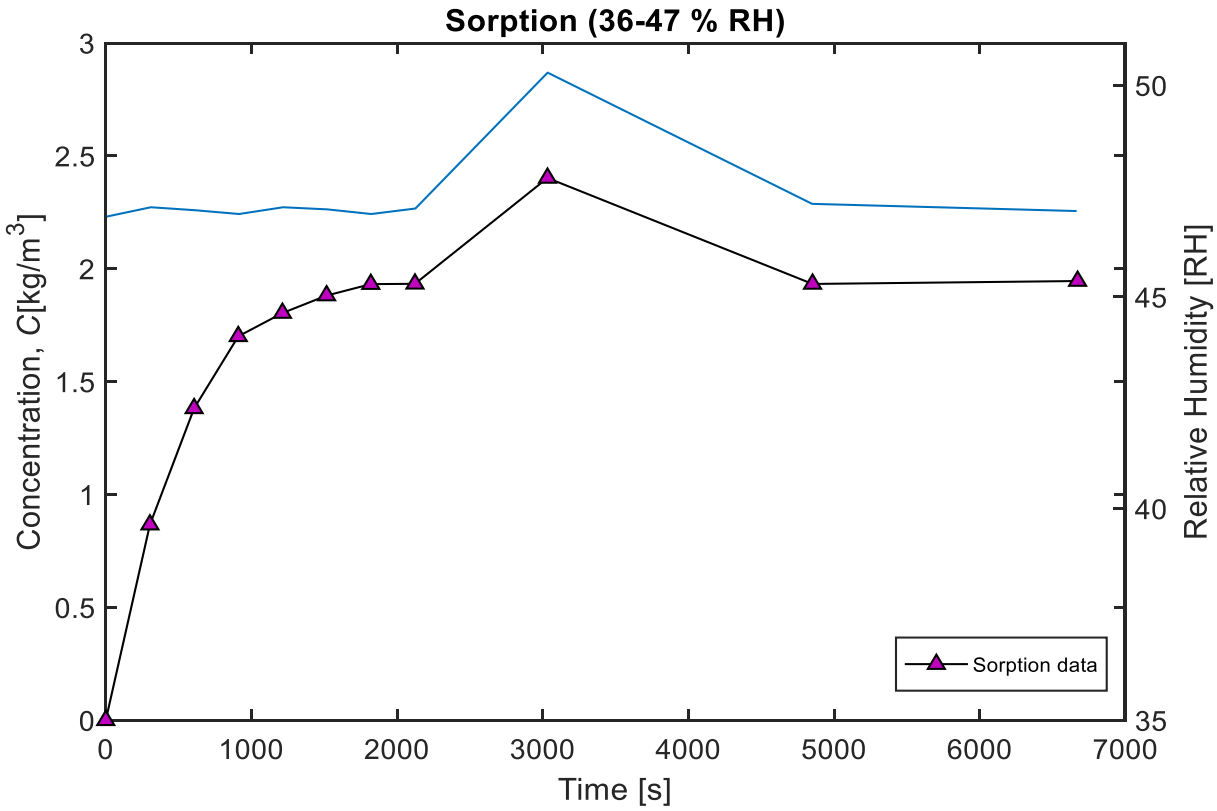

Figure C.1. Sorption/desorption at 30℃ with changing humidity

D. Exposure to Humid Air after Drying

The exposure to humid air between drying and the initial measurement was analysed to understand the influence on dry weight and solubility coefficients. The exposure time was three minutes (time for vacuum chamber to reach surrounding pressure after opening the air valve) for all three samples, however, the humidity varied between 10. 3 % RH and 23.8 % RH. To understand the influence of exposure time and humidity, diffusion coefficients and equilibrium concentrations were calculated at 10 and 24 % RH. This was done by the linear regression given in section 4.1.1 and equilibrium concentrations at given in appendix G, respectively, for given humidity. Absorbed amount of water during exposure could then be determined from eq. 8 and 9. The resulting values are presented in table D.1. The resulting concentration increase during the exposure to 10 % RH and 24 % RH was 0.026 $\frac{kg}{m^3}$ and 0.15 $\frac{kg}{m^3}$, respectively. Exposure at 24 % RH resulted in a concentration increase of approximately 10 % of the equilibrium concentration at 14 % RH, given in appendix G. This suggested that the exposure period is most likely to contribute to deviations over the first humidity step.

Table D.1. Relation between humidity during exposure and water uptake

Exposure time [s]	Humidity during exposure [%]	Diffusion coefficients [m/s^2]	Dimensionless parameter, G	Equilibrium water concentrations [kg/m^3]	Water uptake during exposure [kg/m^3]
180	10	$4.58E^{-13}$	0.0342	0.77	0.026
180	24	$1.02E^{-12}$	0.0616	2.4	0.15

E. Time Dependent Polarization

In contrast to CB-coated conducting polyesters, polymers are generally considered dielectrics. When subjected to an electric field, dielectrics tends to polarize, causing impermanent alignment of charges within the material. Some of charges adjacent to the electrodes cancels out the charges which it set up by the voltage potential across the dielectric, increasing the electric flux density. This can be seen in eq. E1:

$$D = D_0 + P = \varepsilon_0 E + P \qquad (E1)$$

where P and D_0 are the contributions to electric flux density, provided by the polarization and flux at vacuum, respectively. [8]

Polarization may occur momentary or slowly dependent on the mechanisms causing polarization phenomena. However, the slow relaxation mechanisms tend to cause a delay in steady state current. The delay is represented by a time constant τ which is proportional to the relative permittivity and inversely proportional to conductivity of a dielectric: [34]

$$\tau = \frac{\varepsilon_r \varepsilon_0}{\sigma} \qquad (E2)$$

The current as a function of time can then be related to the dielectric time constant through:

$$i(t) = \left(J_\delta(t) + \frac{P_d(\infty)}{\tau} e^{\frac{-t}{\tau}} + \sigma E\right) A \qquad (E3)$$

where $P_d(\infty)$ is the flux contribution from the slow polarization mechanisms over infinite time and J_δ(t)A is the amount of charge abruptly supplied, caused by momentary polarization mechanisms. Stable current is given by the conductivity of the material and provided after some time. [8] A typical curve for the time dependent current with polarization mechanisms can be seen in figure E.1.

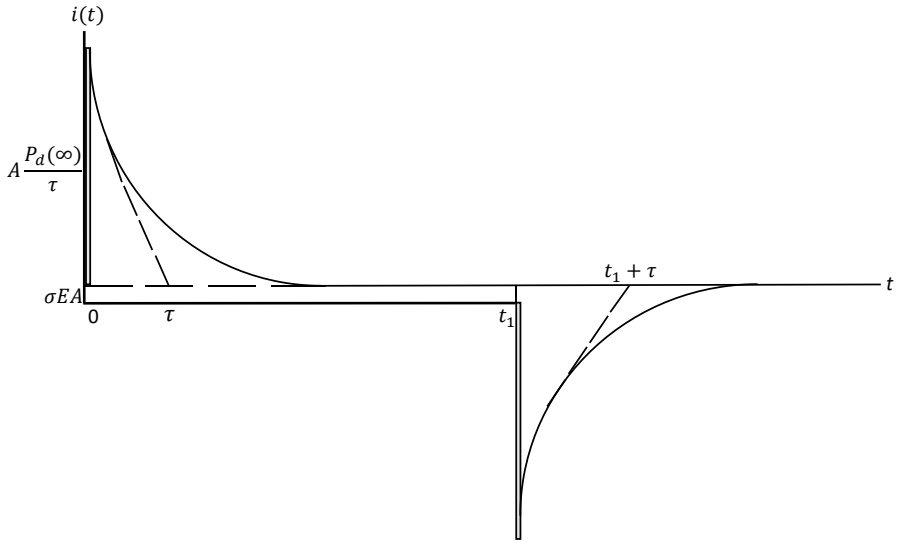

Figure E.1. Contributions to time dependent current and determination of time constant τ. [8] Discharge is occurring at t_1

F. Voltage as a Function of Current

The voltage as a function of current was measured to investigate the tape's electric response to current changes. The measurements were performed according to section 3.2.3 in both radial and axial directions. In order to get the extremities, measurements were performed with weight set 1 and 5. The humidity was set to 20 % and 80 % RH. The correlation between humidity and water concentration can be seen in table 5. Figure F.1 shows the average radial voltage over three distinct samples with corresponding sample deviations. The figure shows a voltage that increases linearly with current, indicating a that the tape acts as an ideal resistor over the range studied. This applied for both measurement directions, weight sets and both humidities. The figure additionally shows that the resistivity decrease is a result of decreasing resistance at high humidity.

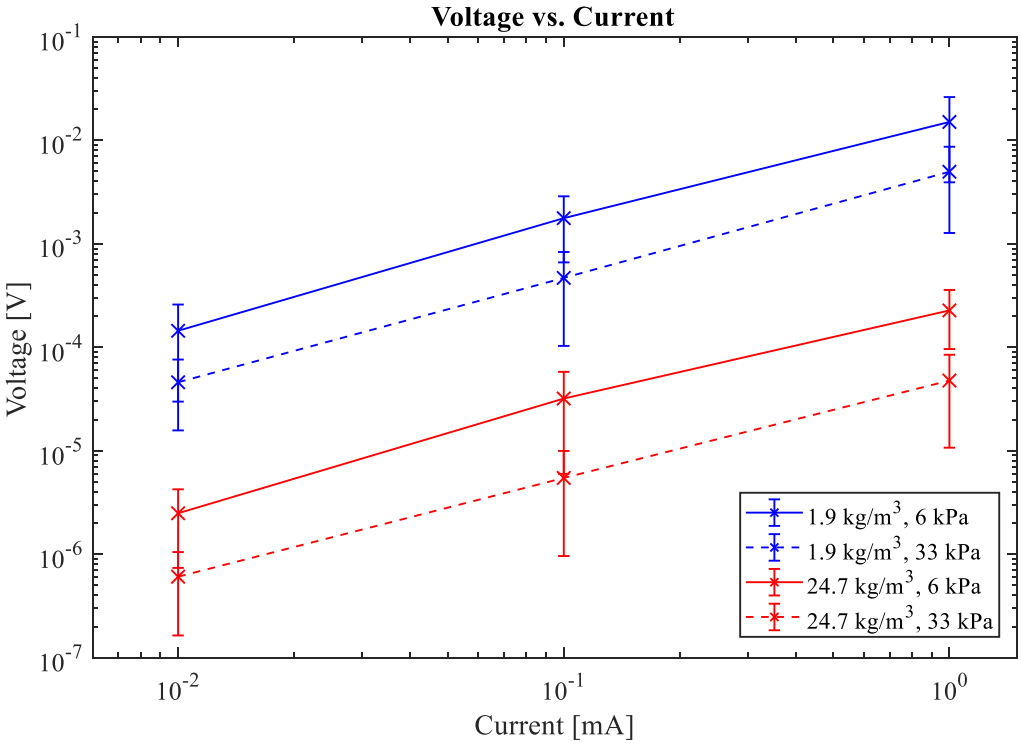

Figure F.1. Voltage as a function of current for a swelling tape

G. Water Concentration

To relate resistivity to water concentration within the tape, the total concentration at various vapor pressures was estimated from the experimental sorption data and determined by fittings of eq. 9. The results can be seen in figure G.1 with regression line $C = a_C e^{b_C p} + c_C e^{d_C p}$ and corresponding constants given in table G.1. y and x represents total concentration and vapor pressure, respectively. Through an exponential regression and eq. 19 it was possible to determine the water concentrations at 20 %, 40 %, 60 % and 80 % RH in subsequent resistivity measurements.

Table G.1 Concentration coefficients as a function of vapor pressure

Vapor Pressure, p [Pa]	a_C	b_C	c_C	d_C
593-3391	7448	0.0004684	-7448	0.0004682

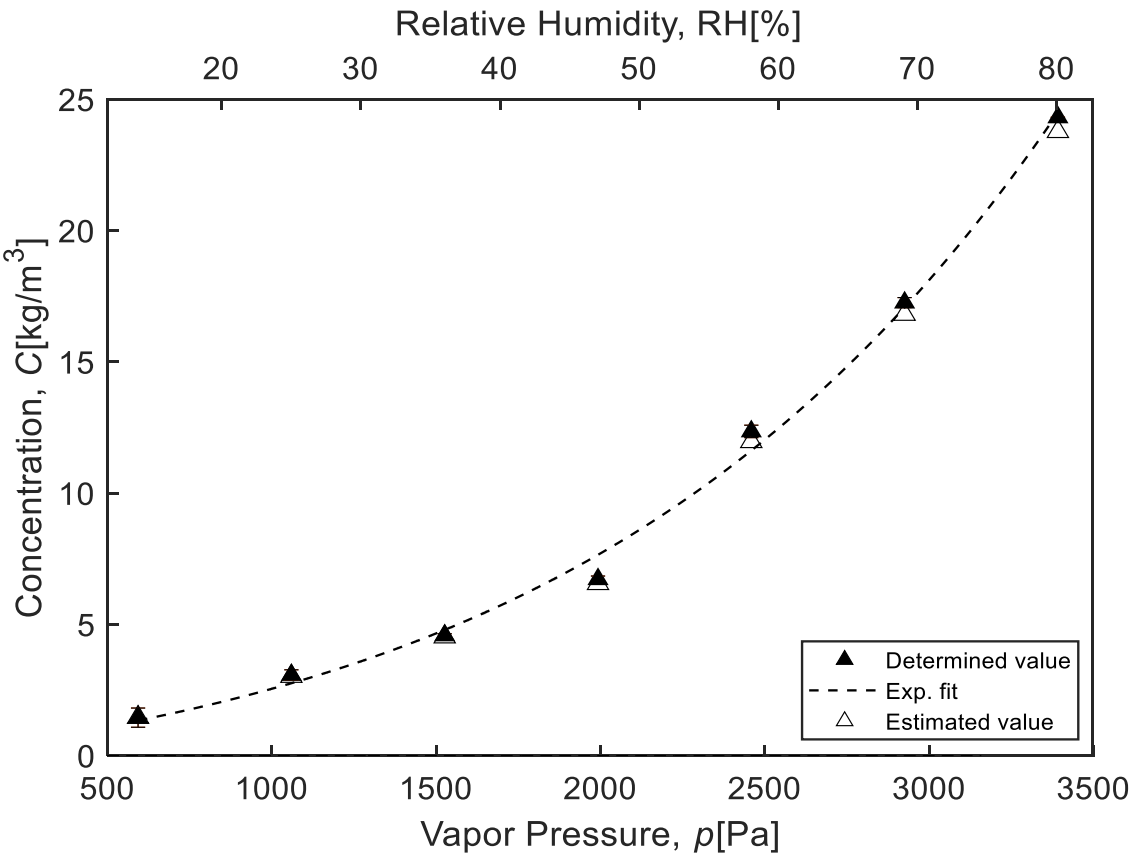

Figure G.1. Sorption/desorption at 30℃ with changing humidity

H. Sample Deviations

Figure H.1 shows the resistivity of four samples after removal of the sample with a deviating resistivity. The resistivity is plotted as a function of mechanical compression and measured with four concentrations of water. A comparison of figure H1 with figure 22 clearly shows a reduction in sample deviation, suggesting that deviations were attributed the inhomogeneity of swelling tapes rather than the measurement method and its apparatus.

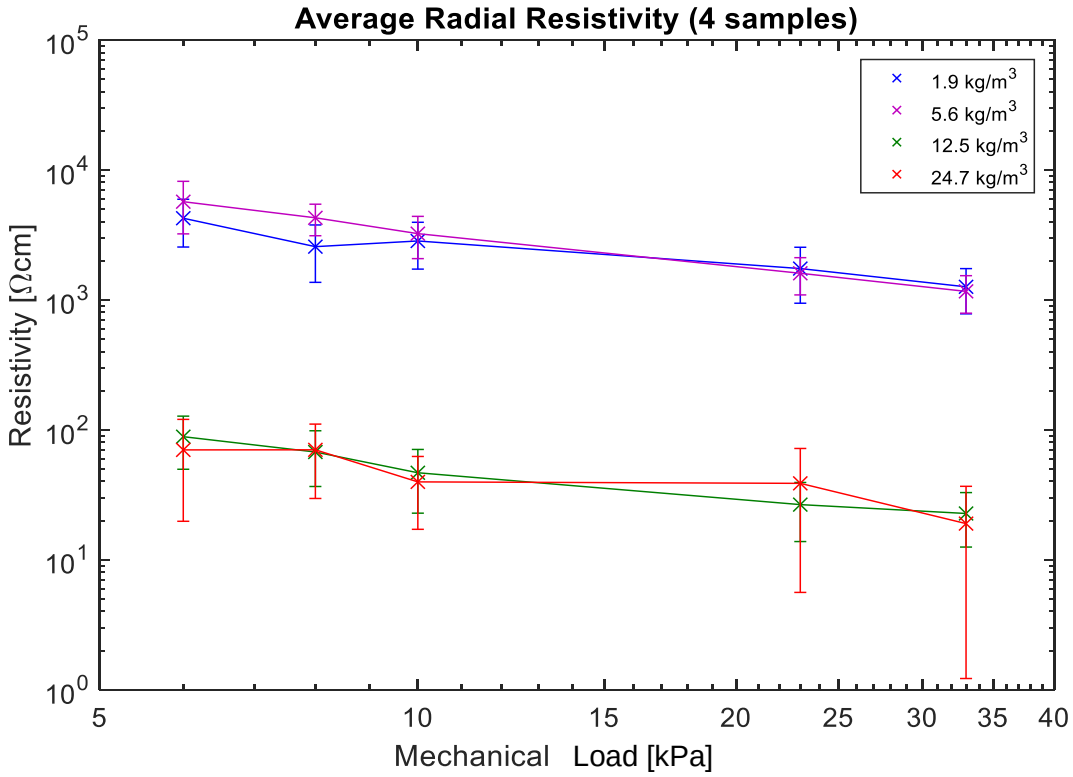

Figure H.1. Resistivity of four samples as a function of mechanical load

I. Microscopy

Microscopy of two samples was performed in order to characterize the topology of a sample showing large deviations in resistivity. Microscopy was done at 21 % RH using a VMX 500 Keyence digital microscope. Images were taken over the exact same areas of the two samples with 20 x zoom. The images cover three areas of the sample's midsection, as seen in figure I.1-6. From the images I.1-6 a slightly higher density of SAP particles was observed for the sample showing higher resistivity (sample 5). A larger SAP area could contribute to increased resistivity by reducing the contact between the upper electrode and the CB coated textile. A larger density of SAPs, hence larger density of ions, could additionally explain the increased reduction in resistivity observed with higher water concentrations of the concerning sample.

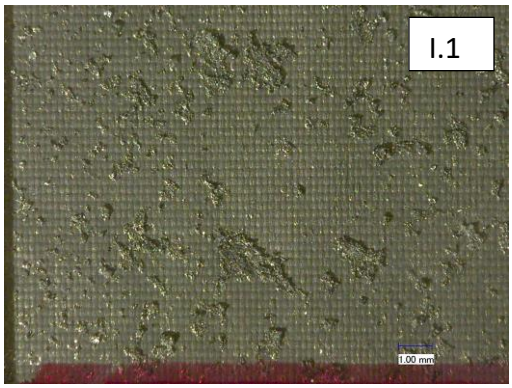

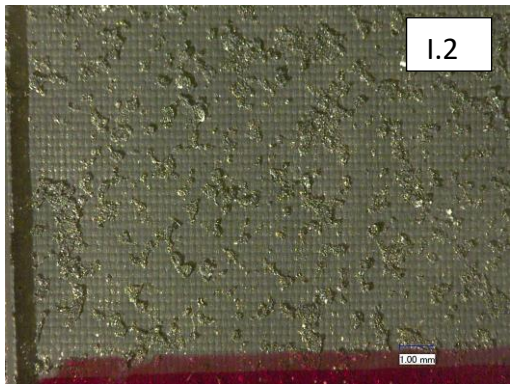

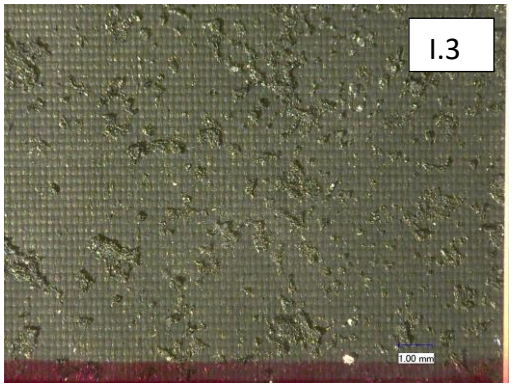

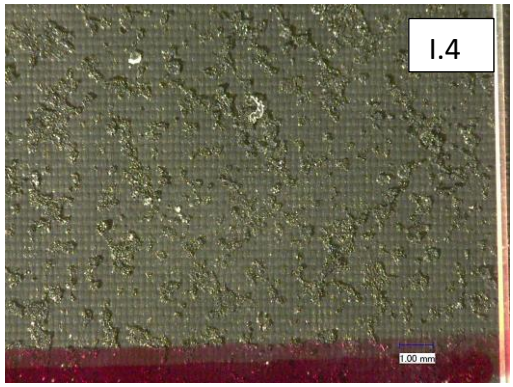

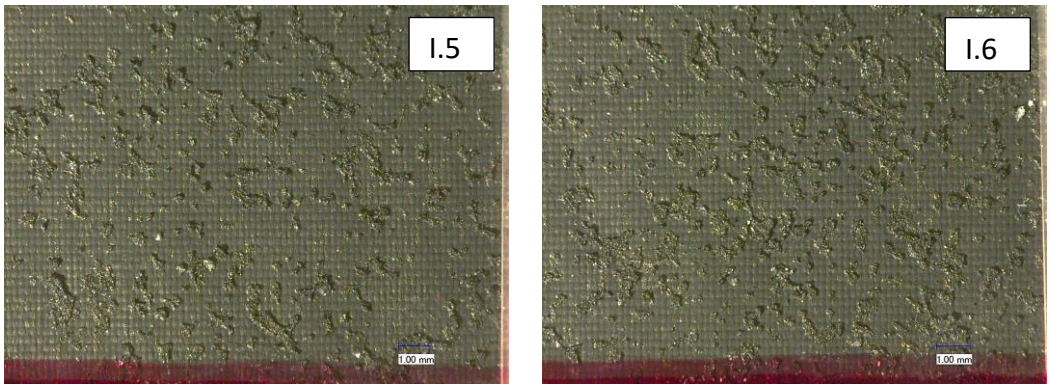

Figure H.1-6. Microscopy at 20 x zoom of sample 3 (left) and sample 5 (right).